TECHNISCHE UNIVERSITÄT WIEN
Vienna University of Technology

Diplomarbeit

Quantitative X-ray fluorescence analysis of samples with various matrices using a universal data evaluation software

ausgeführt am

Atominstitut
der Technischen Universität Wien

Stadionallee 2
1020 Wien

unter Anleitung von

Ao. Univ. Prof. Dipl.-Ing. Dr. Christina Streli
Ao. Univ. Prof. Dipl.-Ing. Dr. Peter Wobrauschek

durch

Philipp Necker, BSc

Josef Klieber Straße 4
2500 Baden

27. April 2017

Kurzfassung

Die Röntgenfluoreszenzanalyse (XRF) ist eine zerstörungsfreie Methode zur Analyse von Elementen und Verbindungen. Sie basiert auf der Emission von charakteristischen Röntgenstrahlen infolge der Bestrahlung einer Probe mit hochenergetischen primären Röntgenstrahlen. Die emittierten Photonen-Energien entsprechen der Energiedifferenz der in dem Prozess involvierten Orbitale, welche charakteristisch für jedes Element und tabelliert sind. Anhand dieser charakteristischen Energien lassen sich die Elemente bestimmen. Damit erhält man die qualitative Analyse der in der Probe enthaltenen Elemente. Das gemessene Spektrum sämtlicher Fluoreszenzlinien ermöglicht nicht nur qualitative Analyse, sondern auch durch Bestimmung der Linienintensitäten, die proportional zur Masse (Konzentration) der entsprechenden Elemente sind, die quantitative Analyse.

Ein bedeutender Teil der vorliegenden Masterarbeit waren Verbesserungen des bereits bestehenden BGQXRF Software-Pakets zur quantitativen Röntgenfluoreszenzanalyse von Bernhard Grossmayer aus dem Jahre 2009 [1]. Die vorgenommenen Änderungen umfassen Benutzeroberflächen-Verbesserungen, sowie erweiterten Funktionsumfang zur besseren Benutzerfreundlichkeit. Das neue BGQXRFPN Software-Paket wird mit einem neuen Report-Design geliefert und ist in 32 und 64-bit erhältlich.

Damit der modulare Aufbau der originalen Software erhalten bleibt, wurden die von Bernhard Grossmayer verwendeten Klassen weiterverwendet. Um das Ziel der maximalen Benutzerfreundlichkeit zu erreichen, weist das verbesserte Software-Paket eine leicht geänderte Struktur auf, welche in Kapitel 3 diskutiert wird.

Um die Benutzerfreundlichkeit und die Verlässlichkeit des BGQXRFPN Software-Pakets zu testen und verifizieren, wurden einige Messungen von Messing- und Bronze-Standards, sowie einem Glass-Standard durchgeführt. Die Messungen beinhalteten mehrere Standard Reference Materials (1103, 1107, 1108 und 621), zertifiziert von National Institute of Standards and Technology (NIST), als auch einige ATI Bronze-Standards (90/4/2/4 und 79.5/12/0.5/8) und wurden an einem TRACOR Spectrace 5000 EDXRF Spektrometer durchgeführt.

Abstract

The X-ray fluorescence analysis (XRF) is a non-destructive analytical technique for elemental and chemical analysis. This method is based on the emission of characteristic X-rays after radiating a sample with high-energetic primary X-ray beams. The emitted photon energies are equal to the energy differences of the involved orbitals. Due to the different electronic orbitals, each element has characteristic fluorescence energies, which are tabulated. With this characteristic energies the elements can be determined. Hence, a qualitative analysis of the included elements of a sample can be performed. The measured spectrum of the fluorescence lines allows by determining the line intensities, which are proportional to the mass (concentration) of the corresponding elements, a quantitative analysis besides the qualitative analysis.

A considerable part of this Master's thesis were improvements of the already existing BGQXRF software package for quantitative X-ray fluorescence which was released in 2009 by Bernhard Grossmayer [1]. The changes included graphical user interface improvements, comprehensive key additions and functionalities for a better user experience. The new BGQXRFPN software package also provides a new design of the report files and is delivered in 32 and 64-bit.

In order to maintain the modular design of the original software, the classes implemented by Bernhard Grossmayer were reused. To achieve the goal of maximum usability, the improved software package has a slightly different structure discussed in chapter 3 of this thesis.

To verify and test the usability and reliability of the BGQXRFPN software package several measurements of brass, bronze and glass standards were performed. The measurements include several Standard Reference Materials (1103, 1107, 1108 and 621) certified by the National Institute of Standards and Technology (NIST), as well as two ATI bronze standards (90/4/2/4 and 79.5/12/0.5/8) and were performed on a TRACOR Spectrace 5000 EDXRF spectrometer.

Contents

1. Physical principles

1.1. Interaction of radiation with matter

If an X-ray beam of a given intensity I_0 passes an absorber with a given thickness x, the radiation will interact with the atoms of the absorber. The result is a reduction of the primary intensity I_0 according to the Beer-Lambert law:

$$I(x) = I_0 \cdot e^{-\mu \cdot x} = I_0 \cdot e^{-(\frac{\mu}{\rho}) \cdot \frac{m}{F}} = I_0 \cdot e^{-(\frac{\mu}{\rho}) \cdot \rho \cdot x} \tag{1.1}$$

μ: linear absorption coefficient $[cm^{-1}]$
$\frac{\mu}{\rho}$: massabsorption coefficient $[cm^2 \cdot g^{-1}]$

The linear absorption coefficient μ is defined by:

$$\mu = \tau + \sigma_{coh} + \sigma_{inc} \tag{1.2}$$

The massabsorption coefficient $(\frac{\mu}{\rho})$ is defined analogously to the linear absorption coefficient:

$$\frac{\mu}{\rho} = \frac{\tau}{\rho} + \frac{\sigma_{coh}}{\rho} + \frac{\sigma_{inc}}{\rho} \tag{1.3}$$

The linear absorption coefficient as well as the massabsorption coefficient depend on the energy of the radiation, the density and chemical composition of the absorber.

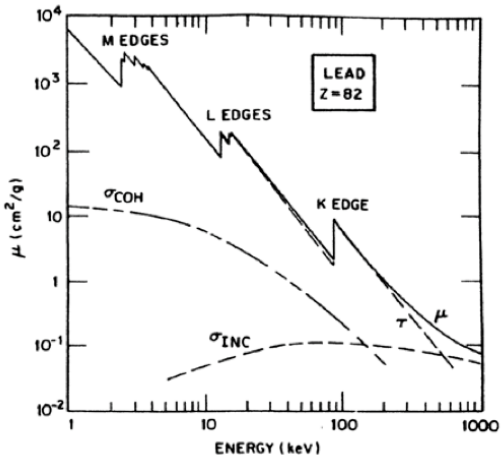

Figure 1.1.: Massabsorption coefficient of Pb as a function of energy [2].

The following interaction types are reducing the intensity of the X-ray radiation as shown in Figure 1.2:

- Photoelectric effect (τ)
- Elastic scattering (σ_{coh})
- Inelastic scattering (σ_{inc})
- Pair production (χ)

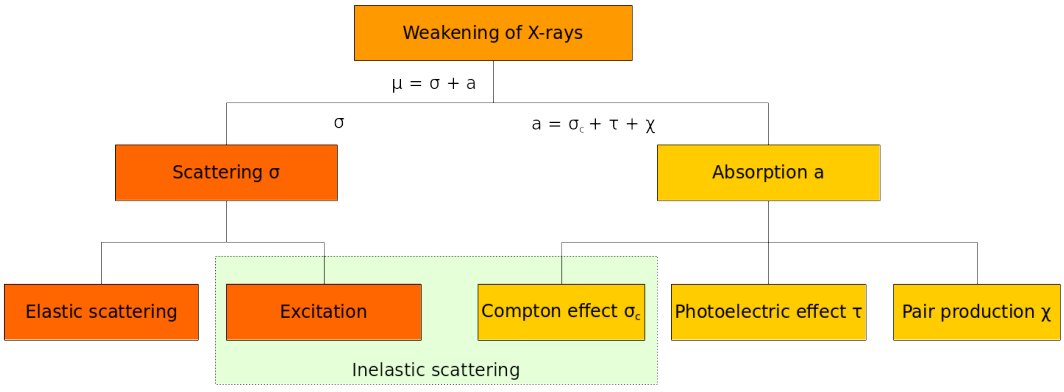

Figure 1.2.: Schematic illustration of the interaction types of X-rays with matter.

1.1.1. Photoelectric effect

The photoelectric effect describes the emission of electrons from the atomic shell in response to incidence light. The emitted electrons are called *photoelectrons*.

This effect has been discovered in 1887 by Heinrich Hertz and could be explained theoretically in 1905 by Albert Einstein. In the following years Robert Millikan's famous experiment could confirm the explanation of this effect experimentally. In 1921 Albert Einstein received the Nobel Price for the correct explanation of the photoelectric effect and two years later Millikan also got the Nobel Price for his work on the photoelectric effect and the elementary charge of electricity.

During the process of the photoelectric effect, photons are getting fully absorbed by the photoelectrons. The surplus energy of the incident photon (after subtracting the binding energy of the photoelectron) is kept by the photoelectron as kinetic energy:

$$E_{kin} = h\nu - E_K - W \tag{1.4}$$

With $hv > E_b$

E_{kin}:	kinetic energy of the photoelectron
$h\nu$:	kinetic energy of the incident photon
E_K:	electron energy of the specific atomic shell (K-shell in this case)
W:	work function
E_b:	binding energy

After the emission of the excited electron the emerged hole will be filled by an electron from a higher shell. This process causes the emission of characteristic X-ray radiation which is also called fluorescence radiation. The energy of the emitted fluorescence photon is then given by the energy difference between the two shells (for example K- and L-shells):

$$E_{ph} = E_L - E_K \tag{1.5}$$

E_{ph}:	kinetic energy of the emitted photon
E_L:	binding energy of the L-shell
E_K:	binding energy of the K-shell

Note that not all transitions from one quantum state to another are possible according to the *transition rules*. These transition rules constrain in following manner:

$$\Delta n \neq 0 \tag{1.6}$$

$$\Delta l \pm 1 \tag{1.7}$$

$$\Delta m = 0, \pm 1 \tag{1.8}$$

The photoelectric absorption coefficient τ, which is the sum of all photoelectric absorption coefficients for each atomic shell, gives the probability of a photoelectric interaction:

$$\tau = \tau_K + (\tau_{L1} + \tau_{L2} + \tau_{L3}) + (\tau_{M1} + \tau_{M2} + \tau_{M3} + \tau_{M4} + \tau_{M5}) + ... \tag{1.9}$$

According to this formula the photoelectric absorption is made up from the absorption in the K shell, the three L shells, the five M shells and so on.

1.1.2. Elastic scattering

Scattering is a process where the incident X-ray radiation interacts with the electrons of the target material. These scattering processes can be distinguished into two main processes: elastic scattering and inelastic scattering.

Elastic scattering implies that no energy is lost during the scattering process which means that the incidence X-ray beam remains at the same wavelength after the interaction with the target atoms. The incident beam as an electromagnetic wave interacts with the electrons of the target. These electrons oscillate with the same frequency as the X-rays and will therefore emit electromagnetic waves with the same frequency. For this reason, the process of elastic scattering is also called coherent scattering or Rayleigh scattering.

The intensity of elastic scattering is dependent on the energy of the incoming electromagnetic wave and the number of electrons which are bound to the atoms of the target. This is basically described by the atomic scattering function describing the electron density of the atom.

1.1.3. Inelastic scattering

In the process of inelastic scattering, also called incoherent scattering or Compton scattering, a certain amount of energy is lost. If a photon hits a loosely bound target electron and recoils it, kinetic energy is transferred from the photon to the electron. The incidence photon will be deflected under a slightly changed wavelength which can be expressed by the following equation:

$$\Delta\lambda = \lambda' - \lambda_0 = \lambda_c(1 - \cos\theta) \tag{1.10}$$

λ_0: wavelength of the incident beam
λ': wavelength of the incoherently scatted beam
λ_c: Compton wavelength $\frac{h}{m_e c}$
θ: angle over which the photons are scattered

At $\theta = 0°$ in Eq. (1.10) $\Delta\lambda$ vanishes and therefore the wavelength remains the same. At $\theta = 180°$ the change of the wavelength reaches a maximum. Note that most of the commercial spectrometers scatter under an angle of $\theta = 90°$, which means that the change of the wavelength remains at $\lambda_c \approx 0.024$ Å compared with coherent scattering. In other words, the angular distribution of the incoherent scattering can be easily predicted. Due to the divergence of the incident X-ray beam, coherent scattering will not only be taking place under a single scattering angle but a distribution of angles. Therefore, also the Compton peak has a wide shape.

The inelastic scattering process can also be written in form of an energy relation:

$$E' = \frac{E}{1 + \alpha \cdot (1 - \cos\theta)} \quad \text{with} \quad \alpha = \frac{E}{m_e c^2} \tag{1.11}$$

E: primary photon energy
E': energy of the inelastic scattered photon
$m_e c^2$: rest energy of the electron

1.1.4. Pair production

The pair production is the main interaction type for photons of high kinetic energy (> 1 MeV). During this process the incident photon will be converted into an electron-positron pair in the near of the atomic nucleus. This can only happen if the kinetic energy of the photon is at least the size of the rest mass energy of the electron-positron pair. Therefore, the minimal energy has to be 2×511 keV $= 1.022$ MeV. As this energy level is far beyond energies used in X-ray fluorescence analysis, it is not relevant during this thesis.

1.1.5. Auger effect

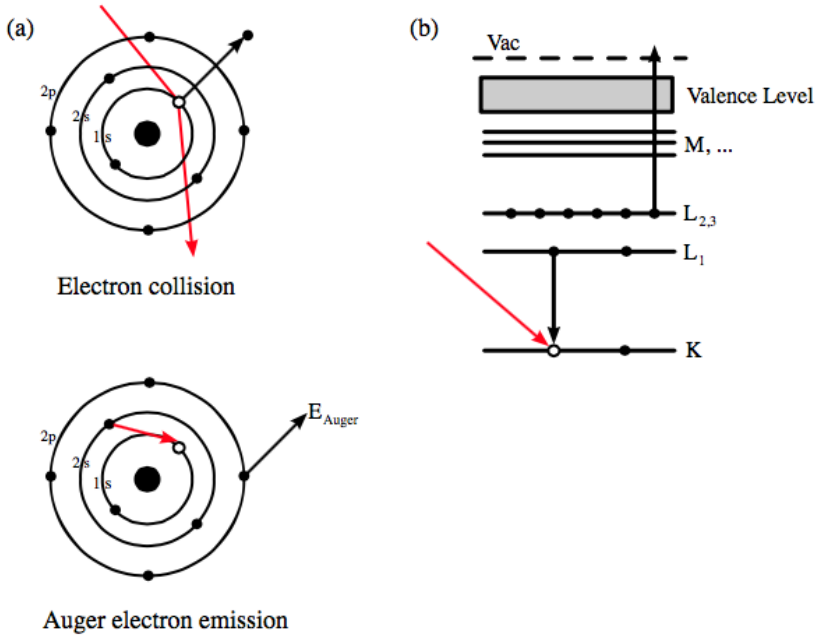

Figure 1.3.: Schematic illustration of the Auger effect. (a) shows the steps involved in the Auger electron emission. (b) represents the process in spectroscopic notation. [3]

The Auger effect is the most competitive process during XRF analysis, because of its lowering effects to the fluorescence yield. It is also one of the main reasons why the analysis of light elements is hard to perform. The Auger effect was discovered by Lise Meitner and first published in 1922 [4]. The effect is named after Pierre Victor Auger who also discovered the effect one year later and independently from Meitner.

During the Auger effect an incident photon hits an inner shell electron and removes it. The left behind vacancy gets filled by an electron from a higher energy level. The released energy during the fill of the vacancy can get transferred to another shell electron which gets ejected from the atom. This electron is called *Auger electron* and has a characteristic kinetic energy depending on the atom and the energy levels involved. This process is also used during Auger electron spectroscopy.

1.2. Generation of X-ray radiation

1.2.1. Characteristic X-ray emission

Characteristic X-ray emission occurs also by direct interaction of high energy electrons with atomic bound electrons. If electrons of high enough kinetic energy hit and remove the shell electrons of the target material a hole is created after ionization. Electrons from higher energy levels will transition to the risen vacancies and emit photons of element specific characteristic energy. The characteristic energy is equivalent to the energy difference of the involved shells of the atom (e.g. energy difference between K and L shells):

$$h\nu = E_L - E_K \tag{1.12}$$

$h\nu$: photon energy
E_L: L-shell binding energy
E_K: K-shell binding energy

For example, the $K_{\alpha 2}$ radiation of copper is 8.0279 keV with binding energies of -951.0 eV (L_2-Shell) and -8978.9 eV (K-Shell).

1.2.2. Bremsstrahlung

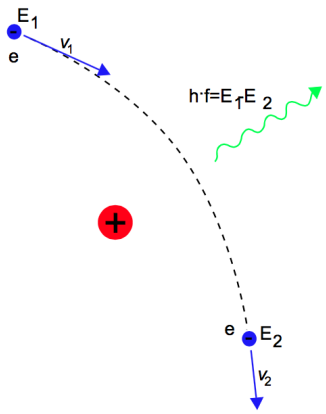

Figure 1.4.: Deflection of an electron in the electric field of an atomic nucleus [5].

The continuous X-ray spectrum, which is getting generated during the deceleration of electrons in the Coulomb field of the atomic nucleus, is called Bremsstrahlung. During this process kinetic energy of an electron is converted into electromagnetic radiation. The energy of the emitted photon can be calculated according to:

$$h\nu = E_1 - E_2 \tag{1.13}$$

$h\nu$: photon energy
E_1: initial electron energy
E_2: final electron energy after the deflection and emission of a photon

The highest possible photon energy can be reached if an electron transfers its whole kinetic energy into photon energy:

$$h\nu = E_1 \tag{1.14}$$

According to the Duane-Hunt law, the maximum energy of the photon implies also the smallest wavelength that can be reached:

$$h\nu = eU \tag{1.15}$$

$$\lambda_{min} = \frac{hc}{eU} \quad \text{with} \quad \lambda = \frac{c}{\nu} \tag{1.16}$$

λ_{min}: minimum wavelength
e: unit load
U: excitation voltage
c: speed of light
h: Planck's constant
ν: frequency

On the basis of formula (1.16), only the excitation voltage U determines the minimum wavelength λ_{min} of the photons.

Formula (1.16) can also be approximated by:

$$E\ [\text{keV}] \approx \frac{1.2396}{\lambda\ [\text{nm}]} \tag{1.17}$$

The continuous intensity distribution of the Bremsstrahlung can be calculated according to the Kramers's rule [6]:

$$J(\lambda) = K \cdot I \cdot Z \cdot \left(\frac{\lambda}{\lambda_{min}} - 1\right) \cdot \frac{1}{\lambda^2} \tag{1.18}$$

J: intensity function
K: Kramers constant
I: electron current
Z: atomic number

1.3. X-ray sources

1.3.1. X-ray tubes

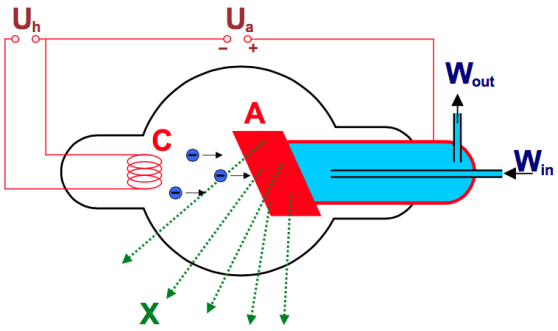

Figure 1.5.: Schematic example of an X-ray tube [7].

The most common way to generate X-rays is using an X-ray tube. Within such a high vacuum tube (10^{-9} bar) made of glass, high voltages are used to accelerate electrons from a hot cathode to an anode. The tube can either be sealed or pumped to create a constant vacuum. The anode is made of a material with a high atomic number. The most common materials used as anodes are copper, molybdenum, rhodium and tungsten. The selection of a target material depends on the intended use of the X-ray tube. For example, in crystallography copper targets are commonly used. The cathode is a filament made of tungsten to serve as an electron source. To focus the electron beam towards the anode, a Wehnelt electrode is used. The acceleration of the electrons is done by creating an electric field where the anode is kept on ground potential while applying a negative potential to the cathode.

The accelerated electrons interact with the anode and produce characteristic and continuous X-ray spectra. The X-ray beam can escape through a small window (usually made of beryllium). Only a small amount of energy used in an X-ray tube is converted into X-rays. Most of the energy is transferred into heat. According to formula (1.15) the maximum amount of energy produced is limited by the exciting voltage.

The energy conversion efficiency η of an X-ray tube is given by:

$$\eta = k \cdot Z \cdot U_A = \frac{I}{i \cdot U_A} \tag{1.19}$$

i: tube current
U_A: anode voltage
Z: atomic number of the anode material
I: X-ray power
k: constant value equal to approximately 10^{-6} kV^{-1}

In a practical setup η is in the order around $0.1 - 1\%$, because of the high amount of heat losses. The maximum electric power is usually between several kW up to 0.1 MW, depending on the working mode and the tube configuration. In medical diagnostics, X-ray tubes are often used in a pulse mode, which could cause problems in the cooling of the anode.

X-ray tubes can be categorized into three different types:

- Low-power tubes < 1 kW (typically around 50 W)
- High-power tubes $1 - 5$ kW
- High-power tubes with rotating anode > 5 kW

The high-power tubes with rotating anodes are commonly used in medical applications or in defectoscopy. In XRF special designs of water cooled rotating anodes up to 18 kW (focus depending) are available on the market.

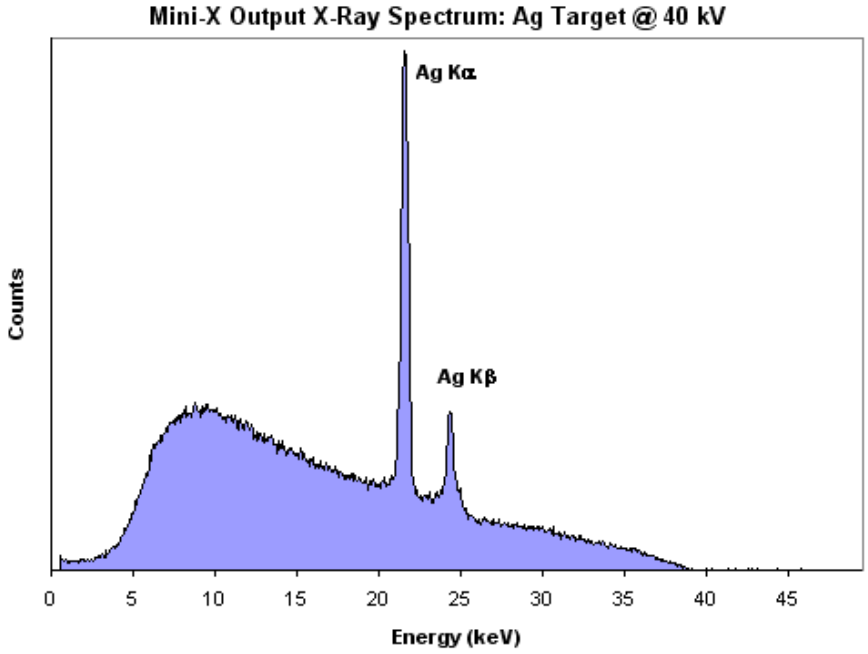

Figure 1.6.: Direct output x-ray spectra from the Mini-X X-ray tube with an Ag target at 40 kV designed by Amptek Inc. [8].

1.3.2. Synchrotron radiation

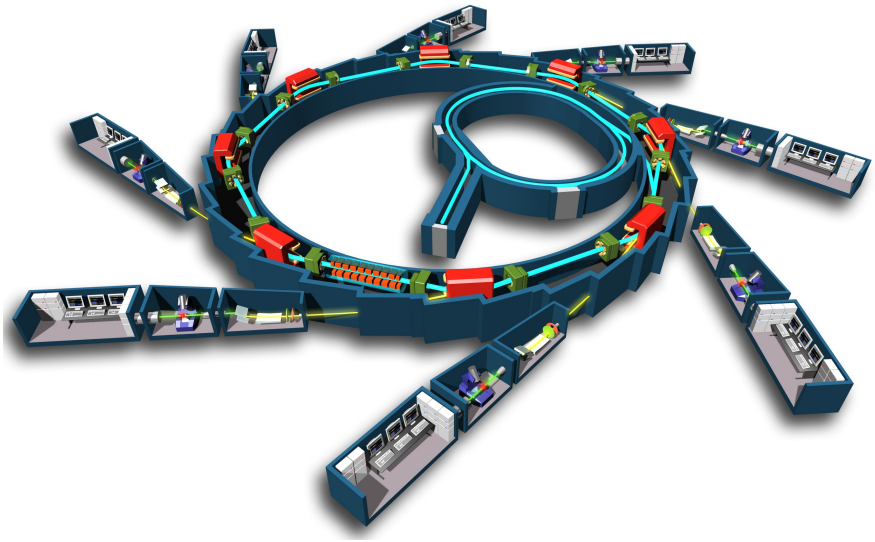

Figure 1.7.: Schematic illustration of the SOLEIL synchrotron facility near Paris, France [9].

Another way to produce X-rays is to use a synchrotron as radiation source. In a synchrotron charged particles are accelerated to relativistic speeds. These particles can be elementary particles or ions. To accelerate and keep the particles on track, electric and magnetic fields are used. Usually the particles get pre-accelerated in linear accelerators and injected after they have reached a kinetic energy around several MeV. The synchrotron radiation is caused by the centripetal forces provided by the magnetic fields which force the particles on the track. These forces represent an acceleration of the particles, therefore resulting in electromagnetic radiation.

Properties of synchrotron radiation include:

- High intensity
- Well defined time structure
- High level of polarization (linear, elliptical or circular)
- Wide spectral range from infrared to X-ray region
- High degree of collimation

To create a constant continuous energy spectrum of synchrotron radiation so-called storage rings are used. These storage rings are synchrotrons where the acceleration of the particles is only used to balance the energy loss after every

rotation. To increase the intensity of the synchrotron radiation, so-called *wigglers* and *undulators* are built into synchrotrons and storage rings.

Wiggler

A wiggler is a set of dipole magnets to periodically deflect a charged particle beam in lateral direction. The emitted synchrotron radiation intensity is much higher than produced in a simple bending magnet and is emitted in the average direction of the particle trajectory. The deflection of the charged particles is much higher than in an undulater, which causes a wider energy spectrum of the emitted radiation. Also the emitted photon energies are higher than in an undulator.

Undulator

An undulator is another setup of periodically arranged dipole magnets. The difference between wigglers and undulaters is the strength of the magnetic field and the resulting energy spectrum. In an undulater, weaker magnets are used to deflect the particles. The electron trajectories are used to interfere with each other to create a smaller energy spectrum and a smaller opening angle. These devices can also be used in free electron lasers.

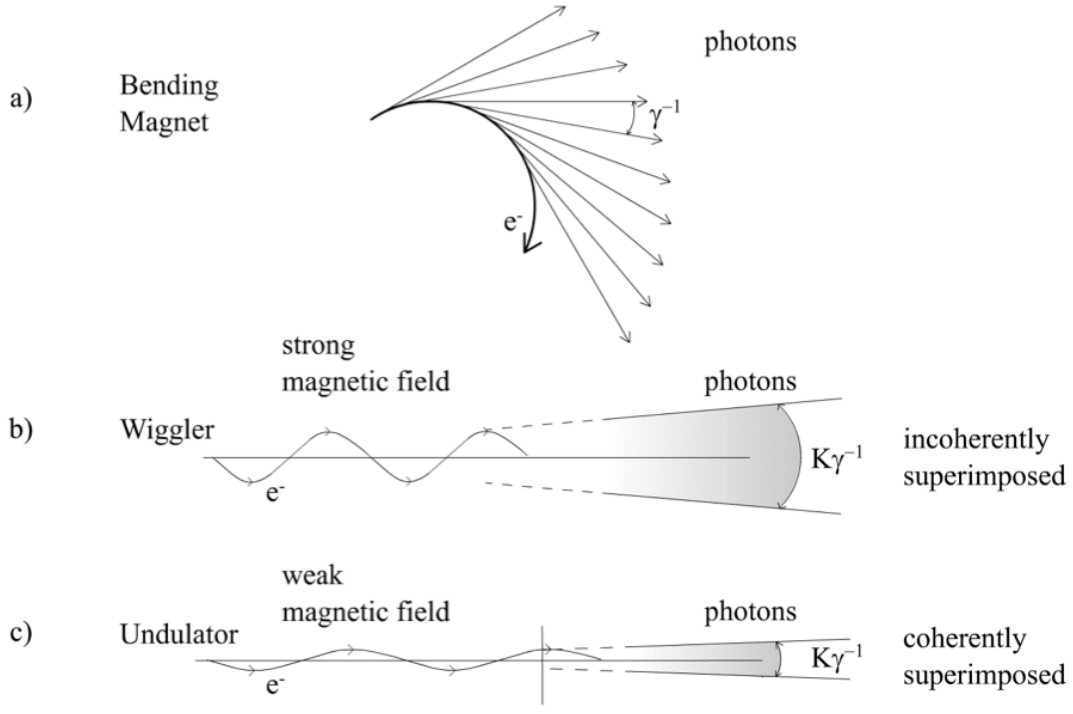

Figure 1.8.: Production of synchrotron radiation with (a) a bending magnet, (b) a wiggler and (c) an undulator [10].

1.4. X-ray fluorescence analysis

The X-ray fluorescence analysis (XRF) is a non-destructive analytical technique for elemental and chemical analysis. Most of the application areas include the analysis of metals, glass and ceramics. The method is based on the emission of fluorescence X-rays after radiating samples with high-energetic X-ray beams. Each element has characteristic fluorescence energies due to the different electronic orbitals. The energy of the emitted photons is equal to the energy difference of the involved orbitals. According to Planck's law, the wavelength of the emitted fluorescence radiation is given by:

$$\lambda = \frac{hc}{E} \tag{1.20}$$

Advantages of X-ray fluorescence analysis:

- Non-destructive method
- Samples can be solid, liquid or gaseous
- Elements from $Z = 5$ to $Z = 92$ can be analyzed

Disadvantages of this analytical technique are:

- Only information from the surface of a sample can be obtained
- No information about chemical bondings

1.4.1. Energy dispersive X-ray fluorescence analysis (EDXRF)

To measure the energy of the emitted characteristic photons, semiconductor detectors are used in EDXRF. During this process, the measurement signals are converted into a signal which is proportional to the measured energies. All energies are detected simultaneously. The energy resolution of the EDXRF is between 600 eV (gas filled) and 200 eV. High resolution setups can reach resolutions up to 125 eV at 5.9 keV (solid state).

1.4.2. Wavelength dispersive X-ray fluorescence analysis (WDXRF)

To separate the wavelengths of the characteristic lines in the wavelength dispersive X-ray fluorescence analysis, crystal spectrometers are used. The diffraction angle θ of the X-rays is defined by Braggs law:

$$n \cdot \lambda = 2d \cdot \sin\theta \tag{1.21}$$

By variation of the angle θ, the wavelength λ of the emitted radiation can be determined. The range of the usable angles is determined through the properties

of the analyzing crystals. The WDXRF has a better energy resolution (between 20 eV and 5 eV) than the EDXRF but is also less efficient. The measurement of the various angles takes significantly more time than the use of a semiconductor detector.

EDXRF	**WDXRF**
Advantages	
Simultaneous measurement	High countrates
Large detection solid angle	Precise quantification
Low power tubes possible	Good energy resolution
Flexible setup	Low spectral background
Disadvantages	
Spectral background	Low solid angle
Worse energy resolution	Sample preparation necessary
Overlapping lines	Line overlaps by higher orders
Reduced detector efficiency	Choice of analyzer crystals

Table 1.1.: Advantages and disadvantages of EDXRF and WDXRF.

1.5. Intensity of the fluorescence beam

1.5.1. Fluorescence radiation through primary excitation

The primary radiation coming from the X-ray source will be reduced by the sample according to the Beer-Lambert law:

$$I(E) = I_0(E) \cdot e^{-\left(\frac{\mu_c(E)}{\rho_c}\right) \cdot \rho_c \cdot \frac{x}{\cos\alpha}} d\Omega_S \tag{1.22}$$

$I_0(E)$: intensity of the primary radiation at energy E
ρ_c: density of the sample
$\mu_c(E)$: linear absorption coefficient of the sample at energy E
$\left(\frac{\mu_c(E)}{\rho_c}\right)$: mass absorption coefficient of the sample at energy E
$d\Omega_S$: solid angle of the emitted radiation from the source

In case of multiple linear absorption coefficients and densities μ_c and ρ_c can be written as:

$$\mu_c(E) = \sum_i \mu_i(E) \cdot c_i \tag{1.23}$$

$$\frac{\mu_c}{\rho_c} = \sum_i \frac{\mu_i \cdot c_i}{\rho_i} \tag{1.24}$$

c_i: concentration of element i
$\mu_i(E)$: linear absorption coefficient of the sample i at energy E
ρ_i: density of the sample element i

The amount of incoming photons which interact through the photoelectric effect with a certain layer and a certain element of a sample is given by:

$$\begin{aligned}\left(1 - e^{-\left(\frac{\tau_c(E)}{\rho_c}\right) \cdot \rho_c \cdot \frac{dx}{\cos\alpha}}\right) \cdot \frac{\left(\frac{\tau_i(E)}{\rho_i}\right)}{\left(\frac{\tau_c(E)}{\rho_c}\right)} \cdot c_i &\approx \left(\frac{\tau_c(E)}{\rho_c}\right) \cdot \rho_c \frac{dx}{\cos\alpha} \cdot \frac{\left(\frac{\tau_i(E)}{\rho_i}\right)}{\left(\frac{\tau_c(E)}{\rho_c}\right)} \cdot c_i \\ &= \left(\frac{\tau_i(E)}{\rho_i}\right) \cdot \rho_c \cdot \frac{dx}{\cos\alpha} \cdot c_i\end{aligned} \tag{1.25}$$

$\left(\frac{\mu_c(E)}{\rho_c}\right)$: mass absorption coefficient of the sample at energy E
$\left(\frac{\mu_i(E)}{\rho_i}\right)$: mass absorption coefficient of the sample element i at energy E

Where $\tau_c(E)$ and $\left(\frac{\mu_c(E)}{\rho_c}\right)$ are given by:

$$\tau_c(E) = \sum_i \tau_i(E) \cdot c_i \tag{1.26}$$

$$\left(\frac{\mu_c(E)}{\rho_c}\right) = \sum_i \left(\frac{\mu_i(E)}{\rho_i}\right) \cdot c_i \tag{1.27}$$

With the jump ratio r_{ij} of a specific edge j of an element i one can calculate the ionization probability $S_{ij}(E)$ of the j shell. In the following the calculation is shown for K and L shells:

$$r_{ij} = \frac{\tau_i(E_{ij} + dE)}{\tau_i(E_{ij} - dE)} < 1 \tag{1.28}$$

K edge energy < E:

$$\begin{aligned} S_{iK} &= \frac{r_{iK} - 1}{r_{iK}} \\ S_{iL1} &= \frac{1}{r_{iK}} \cdot \frac{r_{iL1} - 1}{r_{iL1}} \\ S_{iL2} &= \frac{1}{r_{iK}} \cdot \frac{1}{r_{iL1}} \cdot \frac{r_{iL2} - 1}{r_{iL2}} \\ S_{iL2} &= \frac{1}{r_{iK}} \cdot \frac{1}{r_{iL1}} \cdot \frac{1}{r_{iL2}} \cdot \frac{r_{iL3} - 1}{r_{iL3}} \end{aligned} \tag{1.29}$$

L1 edge energy < E ≤ K edge energy:

$$\begin{aligned} S_{iL1} &= \frac{r_{iL1} - 1}{r_{iL1}} \\ S_{iL2} &= \frac{1}{r_{iL1}} \cdot \frac{r_{iL2} - 1}{r_{iL2}} \\ S_{iL3} &= \frac{1}{r_{iL1}} \cdot \frac{1}{r_{iL2}} \cdot \frac{r_{iL3} - 1}{r_{iL3}} \end{aligned} \tag{1.30}$$

L2 edge energy < E ≤ L1 edge energy:

$$\begin{aligned} S_{iL2} &= \frac{r_{iL2} - 1}{r_{iL2}} \\ S_{iL3} &= \frac{1}{r_{iL2}} \cdot \frac{r_{iL3} - 1}{r_{iL3}} \end{aligned} \tag{1.31}$$

L3 edge energy $< E \leq$ *L2 edge energy:*

$$S_{iL3} = \frac{r_{iL3} - 1}{r_{iL3}} \tag{1.32}$$

Considering the fact that the emitted fluorescence radiation will be weakened inside the sample according to:

$$e^{-\left(\frac{\mu_c(E)}{\rho_c}\right)\cdot\rho_c\cdot\frac{x}{\cos\beta}} \tag{1.33}$$

as well as the detector will only detect a certain amount of radiation:

$$\frac{d\Omega_D}{4\pi} \tag{1.34}$$

$d\Omega_D$: recognized solid angle of the detector

After adding the detector efficiency $\epsilon(E)$, the emission probability p_{ij} of a specific line and the fluorescence yield ω_{ij} of the ionized shell one can finally define the intensity of the fluorescence radiation:

$$\begin{aligned} I_{ijk}^{prim} =& \frac{d\Omega_D d\Omega_S}{4\pi\cos\alpha}\cdot\epsilon(E_{ijk})\cdot p_{ij}\cdot\omega_{ij}\cdot c_i\cdot \\ & \int_{E_{ij}}^{E_{max}} dE \int_0^d dx\cdot I_0(E)\cdot e^{-\left[\left(\frac{\mu_c(E)}{\rho_c}\right)\cdot\frac{1}{\cos\alpha}+\left(\frac{\mu_c(E_{ijk})}{\rho_c}\right)\cdot\frac{1}{\cos\beta}\right]\cdot\rho_c\cdot x}\cdot \\ & \left(\frac{\tau_i(E)}{\rho_i}\right)\cdot\rho_c\cdot S_{ij}(E) \end{aligned} \tag{1.35}$$

E_{ij}: edge energy of the j edge of the element i
E_{ijk}: energy of the j-k line of the element i
E_{max}: maximum photon energy of the primary spectrum

An integration over x gives another expression of the intensity of the primary radiation:

$$I_{ijk}^{prim} = \frac{d\Omega_D d\Omega_S}{4\pi \cos\alpha} \cdot \epsilon(E_{ijk}) \cdot p_{ij} \cdot \omega_{ij} \cdot c_i \cdot$$

$$\int_{E_{ij}}^{E_{max}} dE \int_0^d dx \cdot I_0(E) \cdot \frac{1 - e^{-\left[\left(\frac{\mu_c(E)}{\rho_c}\right)\cdot\frac{1}{\cos\alpha} + \left(\frac{\mu_c(E_{ijk})}{\rho_c}\right)\cdot\frac{1}{\cos\beta}\right]\cdot\rho_c\cdot d}}{\left[\left(\frac{\mu_c(E)}{\rho_c}\right)\cdot\frac{1}{\cos\alpha} + \left(\frac{\mu_c(E_{ijk})}{\rho_c}\right)\cdot\frac{1}{\cos\beta}\right]\cdot\rho_c} \cdot \tag{1.36}$$

$$\left(\frac{\tau_i(E)}{\rho_i}\right) \cdot \rho_c \cdot S_{ij}(E)$$

In a last step, one can define an absorption factor $A(E)$ and summarize the fundamental parameters to a fluorescence cross section $\sigma_{ijk}(E)$ according to:

$$A(E) = \frac{1 - e^{-\left[\left(\frac{\mu_c(E)}{\rho_c}\right)\cdot\frac{1}{\cos\alpha} + \left(\frac{\mu_c(E_{ijk})}{\rho_c}\right)\cdot\frac{1}{\cos\beta}\right]\cdot\rho_c\cdot d}}{\left[\left(\frac{\mu_c(E)}{\rho_c}\right)\cdot\frac{1}{\cos\alpha} + \left(\frac{\mu_c(E_{ijk})}{\rho_c}\right)\cdot\frac{1}{\cos\beta}\right]\cdot\rho_c\cdot d} \tag{1.37}$$

$$\sigma_{ijk}(E) = p_{ij} \cdot \omega_{ij} \cdot \left(\frac{\tau_i(E)}{\rho_c}\right) \tag{1.38}$$

Finally equation (1.36) can be rewritten as:

$$I_{ijk}^{prim} = \frac{d\Omega_D d\Omega_S}{4\pi \cos\alpha} \cdot \epsilon(E_{ijk}) \cdot c_i \cdot d \cdot \rho_c \int_{E_{ij}}^{E_{max}} dE \cdot I_o(E) \cdot A(E) \cdot \sigma_{ijk}(E) \cdot S_{ij}(E) \tag{1.39}$$

Mono energetic excitation

In case of mono energetic excitation, the integration over the energy in equation (1.39) is obsolete. Therefore, the following equation gives the intensity through primary excitation:

$$I_{ijk}^{prim} = \frac{d\Omega_D d\Omega_S}{4\pi \cos\alpha} \cdot \epsilon(E_{ijk}) \cdot c_i \cdot d \cdot \rho_c \cdot I_o(E) \cdot A(E) \cdot \sigma_{ijk}(E) \cdot S_{ij}(E) \tag{1.40}$$

Infinitely thick samples

Infinitely thick sample can be represented by integrating equation (1.35) from $x = 0$ to $x = \infty$:

$$I_{ijk}^{prim} = \frac{d\Omega_D d\Omega_S}{4\pi \cos\alpha} \cdot \epsilon(E_{ijk}) \cdot c_i \cdot \int_{E_{ij}}^{E_{max}} dE \cdot \frac{I_0(E) \cdot \sigma_{ijk}(E) \cdot S_{ij}(E)}{\left[\left(\frac{\mu_c(E)}{\rho_c}\right)\cdot\frac{1}{\cos\alpha} + \left(\frac{\mu_c(E_{ijk})}{\rho_c}\right)\cdot\frac{1}{\cos\beta}\right]} \tag{1.41}$$

Infinite thick samples are generally defined by the following line dependent criteria:

$$d_{1\%} = \frac{-ln(0.01)}{\left[\left(\frac{\mu_c(E)}{\rho_c}\right) \cdot \frac{1}{\cos\alpha} + \left(\frac{\mu_c(E_{ijk})}{\rho_c}\right) \cdot \frac{1}{\cos\beta} \cdot \rho_c\right]} \tag{1.42}$$

Thick samples are called thick if only 1% of the fluorescence radiation from the sample reaches the surface of the sample. According to the line dependence in equation (1.42), this criteria has to be fulfilled by the element with the highest atomic number of the sample.

Thin film samples

In case of thin film samples the absorption factor A(E) from equation (1.39) changes to:

$$A(E) = lim_{d\to 0} \frac{1 - e^{-a\cdot d}}{a \cdot d} = 1 \tag{1.43}$$

Therefore equation (1.39) can be written as:

$$I_{ijk}^{prim} = \frac{d\Omega_D d\Omega_S}{4\pi \cos\alpha} \cdot \epsilon(E_{ijk}) \cdot c_i \cdot d \cdot \rho_c \int_{E_{ij}}^{E_{max}} dE \cdot I_o(E) \cdot \sigma_{ijk}(E) \cdot S_{ij}(E) \tag{1.44}$$

The intensity of thin film samples is directly proportional to the concentration c_i and is dependent on the fundamental parameters and the measurement system. This can be written with the sensitivity of the measurement system S_{ijk} of the j-k line of the element i and the mass of the sample m:

$$I_{ijk}^{prim} = c_i \cdot S_{ijk} \cdot m \tag{1.45}$$

After the measurement of the relative sensitivity S_{ijk}^{rel} of the intensity of a certain line of a standard element x (with known concentration c_x), one can calculate the concentration c_i of a certain element i within a sample:

$$S_{ijk}^{rel} = \frac{I_{ijk}}{I_{xyz}} \tag{1.46}$$

$$c_i = \frac{I_{ijk}}{I_{xyz}} \cdot \frac{1}{S_{ijk}^{rel}} \cdot c_x \tag{1.47}$$

The definition of a thin film sample is done analogously to the thick sample criteria, however 99% of the fluorescence radiation has to reach the surface of the

sample:

$$d_{99\%} = \frac{-ln(0.99)}{\left[\left(\frac{\mu_c(E)}{\rho_c}\right) \cdot \frac{1}{\cos\alpha} + \left(\frac{\mu_c(E_{ijk})}{\rho_c}\right) \cdot \frac{1}{\cos\beta} \cdot \rho_c\right]} \tag{1.48}$$

1.5.2. Fluorescence radiation through secondary excitation

Primary excited elements can also excite other elements within a sample through their fluorescence radiation. This process is called secondary excitation. In case of thick samples with high concentrations of elements, secondary excitation is expected.

The derivation of the intensity of the fluorescence radiation through secondary excitation has been done by Xavier Gruber within his Master's thesis [11] and is not dealt within this thesis.

1.6. Semiconductor detectors

Semiconductors are materials with an electric conductivity between conductors and insulators. They can either be crystals or amorphous solids. Unlike in metals, the conductivity of semiconductors increases with higher temperature and is dependent on a radiation effect. Due to the radiation dependent conductivity semiconductors can be used as detectors for ionizing radiation. In case of incident radiation, the radiation sensitive part of such a detector generates electron-hole pairs which are deducted towards the poles by an applied voltage. The resulting current is proportional to the energy of the incident photons and can be measured. The amount of charge is given by the following equation:

$$Q = \frac{E}{\epsilon} \tag{1.49}$$

Q: amount of charge
E: photon energy
ϵ: mean energy for the generation of electron-hole pairs

Dependent on the mechanisms involved in the electron-hole generation, the value of ϵ differs among different detectors.

The generation time of the electron-hole pairs ranges from a few picoseconds up to microseconds. The collection time of the carriers is dependent on the mobility of the carriers inside the detector, on the applied fields, and on the traveling distances within the semiconductor. In silicon detectors, this time can be around nanoseconds, in gas-filled detectors up to microseconds.

To increase the conductivity of a semiconductor, the material is usually doped with another sort of atoms. If the foreign atom has one electron more than the used atoms in the material, the semiconductor is called n-doped. In case of one foreign atom electron less, the material is called p-doped. A pn junction can be created if a p- and a n-doped semiconductor are combined. This is called a semiconuductor diode.

1.6.1. PSN- and PIN-diode

A PSN-diode is a semiconductor diode with a weakly doped s-zone between the p- and the n-doped zones. If the s-zone is barely doped (e.g. n-doped), the junction will spread over the whole zone into blocking direction and determine the radiation sensitive volume of the detector.

A PIN-diode has a wide undoped i-zone between the p- and the n-doped semiconductor zones, which is called intrinsic zone. This zone represents a rectifier.

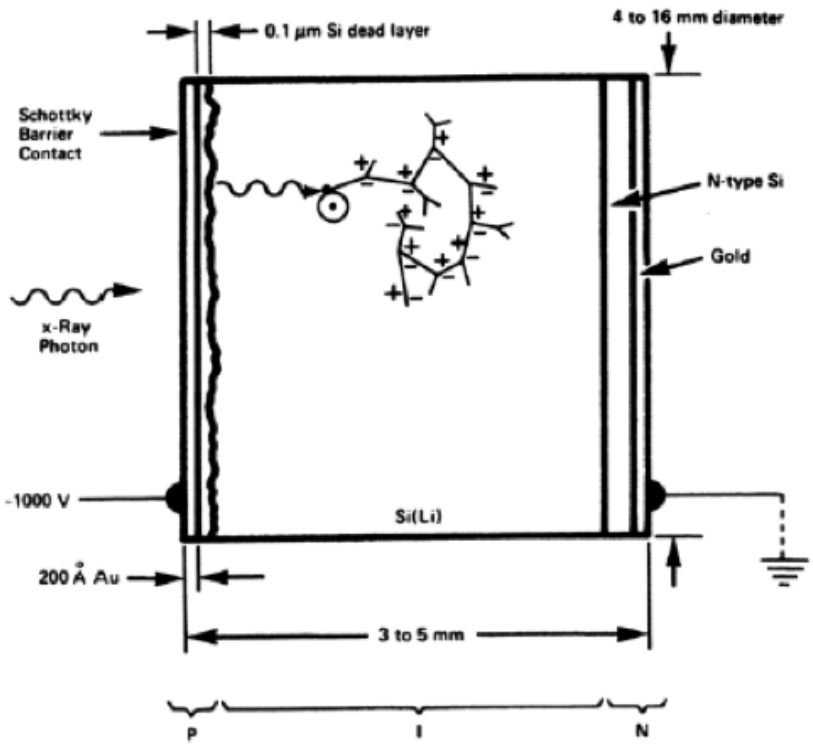

Figure 1.9.: Schematic illustration of a PIN-diode used as a radiation detector [2].

Under operation the intrinsic zone of the detector is flooded with charge carriers from both outer zones. The charge carriers have a very large life time inside this i-zone (τ in the range of μs), therefore PIN-diodes can be used for detection of very short voltage pulses $t_{puls} < \tau$. PIN-diodes can be produced by diffusing lithium ions into a boron doped p-silicon. The concentration of the n-zone decreases into the direction of the bulk and only the surface will remain as a real n-doped zone. By applying a voltage onto the detector, the lithium atoms will drift into the blocking direction and create a zone with a balance of lithium and boron atoms. Analogously to the PSN-diode, the depletion zone of the detector will spread over the i-zone and determine the radiation sensitive volume of the semiconductor detector.

1.6.2. Detector models

Crystal detector

Crystal detectors are the most simple semiconductor detectors. Usually they are made of pure and homogenous germanium or silicon crystals. While germanium detectors can have a radiation sensitive thickness of a few centimeters, silicon detectors can only be built a few millimeters thick. Therefore germanium detectors

can be used for much higher radiation energies up to MeV.

A crystal detector usually consists of a highly pure germanium crystal with vapor deposited layers as electrodes. By applying a voltage, intrinsic conduction and a leakage current occur. To decrease the amount of intrinsic conduction and, hence, the noise, the detectors are cooled with liquid nitrogen. Incoming radiation creates electron-hole pairs which will create a current which overlaps the leakage current and can be measured.

Junction detector

In a junction detector, the space charge free zone of an in blocking direction operated diode is used to detect the incoming radiation. A very small leakage current appears through the junction analogous to a crystal detector. The radiation sensitive layer of the junction detector is smaller than the one in crystal detectors and lets radiation of high energy pass without detection. Besides, the smaller size of the junction layer allows higher voltages and leads to smaller gathering times of the charge carriers.

Lithium drifted detector

A lithium drifted detector is a PIN-diode with a weakly p-doped silicon crystal which has been drifted with lithium atoms from one side. The diffusion is done at temperatures between 300°C and 600°C. After diffusion, the drift of lithium atoms will be done at around 100°C and 200°C and cooled afterwards at room temperature.

In contrast to junction detectors, the radiation sensitive layer is larger which leads to lower time resolution in the detection process.

To reach the active layer of a lithium drift detector, the incoming radiation has to pass a gold contact layer (around 0.02 μm) and a dead layer from the drifting process (around 0.01 μm). Low energetic radiation will be lost by passing these two layers and cannot be detected inside the active layer. During operation the detector has to be cooled with liquid nitrogen to keep the noise level low and to keep the drifted lithium atoms in position in the crystal.

Silicon drift detector

In a silicon drift detector (SDD), highly resistive n-doped silicon is combined with a highly n-doped zone on one side and a highly p-doped zone on the other side. In this kind of PSN-diode, aluminium is used as contact layer.

The main advantage of silicon drift detectors is the possible small anode size, which leads to less noise while detection. These smaller anode sizes are unique for

this kind of detectors and can be established by using sidewards depletion. SDDs have a good energy resolution, high count rates and can be used with Peltier cooling unlike germanium detectors.

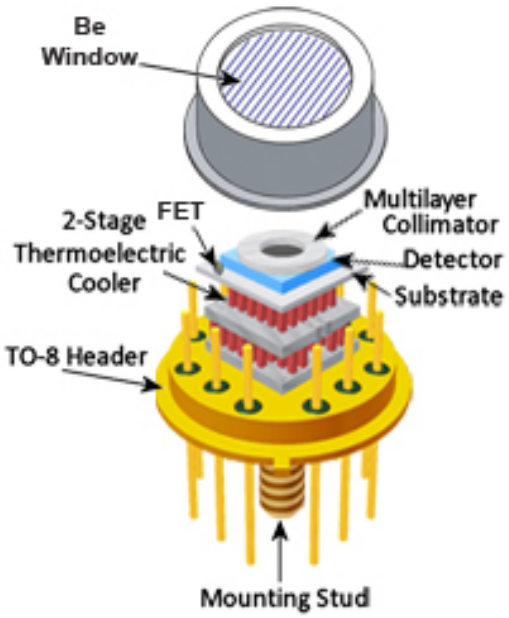

Figure 1.10.: Example of a silicon drift detector [12].

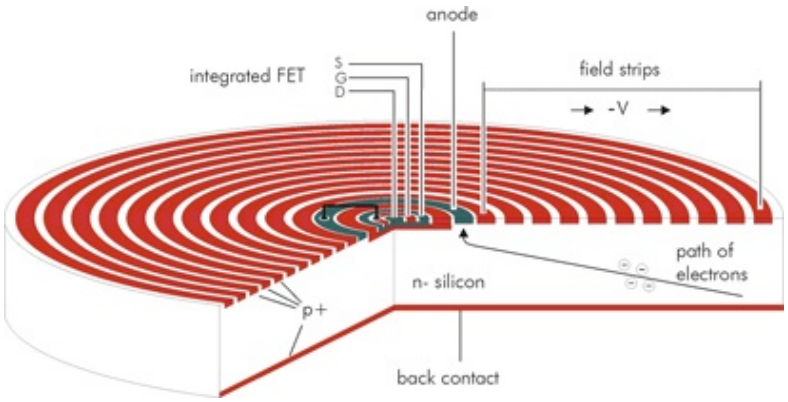

Figure 1.11.: Schematic illustration of a ring shaped silicon drift detector [13].

1.7. Simulation of the X-ray spectrum

Within the BGQXRFPN software package, two simulation methods of the X-ray spectrum are implemented [1]:

- Wiederschwinger [14]
- Love & Scott [15, 16]

1.7.1. Simulation of the continuos spectrum

The frequency distribution of the emitted photons can be calculated according to:

$$\Delta n_E = \sigma \cdot f(\chi) \cdot D_E \cdot \Omega_S \cdot i \cdot t \cdot \Delta E \tag{1.50}$$

The variable σ is dependent on the used simulation model and is given through:

$$\sigma = const \cdot Z \cdot \left(\frac{E_0}{E} - 1\right)^x \tag{1.51}$$

Δn_E:	amount of photons within an energy interval of E and $E + \Delta E$ within a solid angle Ω_S and a measurement time t
E:	photon energy
ΔE:	considered energy interval [keV]
Ω_S:	solid angle of the primary radiation [sr]
t:	measurement time [s]
i:	tube current [mA]
Z:	atomic number of the anode material
E_0:	maximum electron energy [keV] according to $E_0 = e \cdot U$
$f(\chi)$:	self absorption of the emitted radiation within the anode
D_E:	weakening factor of the exit window of the tube and used filters

Wiederschwinger	**Love & Scott**
$const = 1.35 \cdot 10^9$ [$\mathrm{sr^{-1}mA^{-1}keV^{-1}s^{-1}}$]	$const = 1.36 \cdot 10^9$ [$\mathrm{sr^{-1}mA^{-1}keV^{-1}s^{-1}}$]
$x = 1.109 - 0.00435 \cdot Z + 0.000175 \cdot E_0$	$x = 1.0314 - 0.0032 \cdot Z + 0.0047 \cdot E_0$

Table 1.2.: Differences between the Wiederschwinger and the Love & Scott simulation methods according to [14, 15, 16].

According to the Love & Scott simulation model, the maximum generation depth z_m is given through:

$$z_m = \frac{A}{\rho \cdot Z} \cdot (0.787 \cdot 10^{-5} \cdot \sqrt{J} \cdot E_0^{3/2} + 0.735 \cdot 10^{-6} \cdot E_0^2) \tag{1.52}$$

$$J = 0.0135 \cdot Z \tag{1.53}$$

z_m: maximum generation depth [cm]
A: atomic mass of the anode material
J: ionization potential of the anode material [kV]
ρ: density of the anode material $[g \cdot cm^3]$

$$\bar{z} = z_m \cdot \frac{0.49269 - 1.0987 \cdot \eta + 0.78557 \cdot \eta^2}{0.70256 - 1.09865 \cdot \eta + 1.0046 \cdot \eta^2 + ln(U_0)} \cdot ln(U_0) \tag{1.54}$$

$\bar{z}$: mean generation depth [cm]
η: backscattering coefficient of the anode material
U_0: overvoltage

$$U_0 = \frac{E_0}{E} \tag{1.55}$$

$$\eta = E_0^m \cdot e^c \tag{1.56}$$

$$m = 0.1382 - \frac{0.9211}{\sqrt{Z}} \tag{1.57}$$

$$e^c = 0.1904 - 0.2236 \cdot ln(Z) + 0.1292 \cdot (ln(Z))^2 - 0.01491 \cdot (ln(Z))^3 \tag{1.58}$$

$$f(\chi) = \frac{1 - e^{-2 \cdot \chi \cdot \rho \cdot \bar{z}}}{2 \cdot \chi \cdot \rho \cdot \bar{z}} \tag{1.59}$$

$$\chi = \tau(E) \cdot \frac{\cos \alpha}{\cos \beta} \tag{1.60}$$

$\tau(E)$: photoelectric mass absorption coefficient

1.7.2. Simulation of the characteristic spectrum

The number of photons of the characteristic spectrum n_{jk} is given by the following equation:

$$n_{jk} = const \cdot \frac{1}{S_j} \cdot R \cdot \omega_j \cdot p_{jk} \cdot f(\chi_{jk}) \cdot D_{jk} \cdot i \cdot \Omega_S \cdot t \tag{1.61}$$

with $const = 6 \cdot 10^{13}$ [sr^{-1} $\mathrm{mA}^{-1}\mathrm{s}^{-1}$].

n_{jk}:	number of photons from the j-k line within a solid angle Ω_S and a measurement time t
$\frac{1}{S_j}$:	intensity factor
R:	backscatter coefficient of the anode material
ω_j:	fluorescence yield of the j line
p_{jk}:	transition probability of the j-k line
$f(\chi_{ij})$:	self absorption of the emitted characteristic radiation within the anode
D_{jk}:	weakening factor of the j-k line for the exit window of the tube and used filters

The following parameters are used in the Love & Scott model:

$$\begin{aligned}\frac{1}{S_j} =& \frac{z_j \cdot b_j}{Z} \cdot (U_0 \cdot ln(U_0) + 1 - U_0) \cdot \\ & \left[1 + 15.5 \cdot \sqrt{\frac{J}{E_j}} \frac{\sqrt{U_0} \cdot ln(U_0) + 2 \cdot (1 - \sqrt{U_0})}{U_0 \cdot ln(U_0) + 1 - U_0}\right]\end{aligned} \tag{1.62}$$

$$R = 1 - 0.008152 \cdot Z + 3.613 \cdot 10^{-5} \cdot Z^2 + 0.009582 \cdot Z \cdot e^{-U_0} + 0.00114 \cdot E_0 \tag{1.63}$$

Within the Wiederschinger simulation model, the parameters are changed to:

$$\begin{aligned}\frac{1}{S_j} =& \frac{z_j \cdot b_j}{Z} \cdot (U_0 \cdot ln(U_0) + 1 - U_0) \cdot \\ & \left[1 + 16.05 \cdot \sqrt{\frac{J}{E_j}} \frac{\sqrt{U_0} \cdot ln(U_0) + 2 \cdot (1 - \sqrt{U_0})}{U_0 \cdot ln(U_0) + 1 - U_0}\right]\end{aligned} \tag{1.64}$$

$$R = 1 + \sum_{l=1}^{5} \sum_{m=1}^{l} a_{m,l-m+1} \cdot \left(\frac{1}{U_0} - 1\right)^m \cdot Z^{l-m+1} \tag{1.65}$$

$$a_{pq} = \begin{bmatrix} 5.580848699 \cdot 10^{-3} & 2.709177328 \cdot 10^{-4} & -5.531081141 \cdot 10^{-6} & -5.31081141 \cdot 10^{-8} & -3.210316856 \cdot 10^{-10} \\ 3.401533559 \cdot 10^{-2} & -1.601761397 \cdot 10^{-4} & 2.473523226 \cdot 10^{-6} & -3.020861042 \cdot 10^{-8} & 0 \\ 9.916651666 \cdot 10^{-2} & -4.615018255 \cdot 10^{-4} & -4.332933627 \cdot 10^{-7} & 0 & 0 \\ 1.030099792 \cdot 10^{-1} & -3.113053618 \cdot 10^{-4} & 0 & 0 & 0 \\ 3.630169747 \cdot 10^{-2} & 0 & 0 & 0 & 0 \end{bmatrix}$$

a_{pq}: parameter for the calculation of the backscatter coefficient
U_0: overvoltage

$$U_0 = \frac{E_0}{E_j} \tag{1.66}$$

The following applies to the number of electrons within the ionized shell z_j:

$$z_K = 2 \quad \text{and} \quad z_L = 8 \tag{1.67}$$

as well as for b_j:

$$b_K = 0.35 \quad \text{and} \quad b_L = 0.25 \tag{1.68}$$

The self absorption of the emitted characteristic radiation $f(\chi_{ij})$ is defined by:

$$f(\chi_{ij}) = \frac{1 - e^{-2 \cdot \chi_{ij} \cdot \rho \cdot \bar{z}}}{2 \cdot \chi_{ij} \cdot \rho \cdot \bar{z}} \tag{1.69}$$

$$\chi_{ij} = \tau(E_{ij}) \cdot \frac{\cos \alpha}{\cos \beta} \tag{1.70}$$

where E_{ij} represents the energy of the j-k line.

The mean generation depth is calculated according to formula (1.54) with the overvoltage definition from (1.66).

2. About BGQXRFPN

BGQXRFPN is an extension of the already existing BGQXRF software package, which was designed for quantitative X-ray fluorescence analysis. [1]

The updated version provides an improved user interface and delivers some comprehensive key additions and functionalities for a better user experience. Moreover, major bugs have been fixed and the report layout has been changed.

The software packaged has the following updated structure:

- Doc
- elemente
- Filter
- gnuplot
- Output
- Properties
- BGQXRF_PN_32bit.exe
- BGQXRF_PN_64bit.exe
- Elements.xml

The *Doc* folder contains the documentation of the software package. All preset filters delivered in this software package are stored in the *Filter* folder, preset *property files* are located in the *Properties* folder. The *Output* folder can be used as file location for reports. It is the default location of reports generated within the *batch mode* of BGQXRFPN. With this software package the open-source plotting software *gnuplot* is delivered in 32-bit within a folder of the same name.

The BGQXRFPN software itself is delivered in 32 and 64-bit for different CPU architectures with corresponding names.

To launch the software, one has to double-cklick the executable. At startup the program looks for a default *property file* (Properties.xml) and a default *fundamental parameter file* (Elements.xml). If one of this files is missing, a message-box with

a warning will open and inform the user. Missing files can be ignored as long as at least a *fundamental parameter file* is provided before the start of calculation. The use of *property files* within the software package is optional, but recommended.

3. User Interface changes and the main parts of BGQXRFPN

A considerable part of this Master's thesis was the execution of user interface improvements of the already existing BGQXRF software package which was released in 2009 by Bernhard Grossmayer [1].

In this chapter, all major changes from BGQXRF to BGQXRFPN will be presented. Most of the implemented changes are related to the user interface of this software package. Moreover, major bugs have been removed. The main window in the new software package has been changed to a single column tab-view to provide a better overview for the user. New tabs have been created and further functionality has been added. In addition, a new report layout has been implemented.

3.1. Properties

Within this tab of the software package all the buttons have been reordered in the main window. Additional quick-tips have been implemented and positioned besides the corresponding categories. Three categories of settings have been created.

3.1.1. Fundamental Parameters

The *Fundamental Parameters* section contains all the settings related to the calculation method with fundamental parameters. It is possible to choose the fundamental parameters input file format (XML, Darek, Ebel) and the *fundamental parameters file* itself. One can also create a new *fundamental parameters file*, or load a different one. The default file is called *Elements.xml* and is content of the software package.

At the bottom of the *Fundamental Parameters* section is the *autoadjust file locations (for FP and gnuplot)* checkbox. It allows the user to automatically check the file locations of the fundamental parameters file, the gnuplot binary path and the gnuplot binary name at the start of BGQXRFPN. If they cannot be found, the default values of the software will be selected. Unchecking this checkbox after program startup will not take effect for security reasons. Only an imported *property file* will cause the change, if within the *property file* the *autoadjustfiles* option is set.

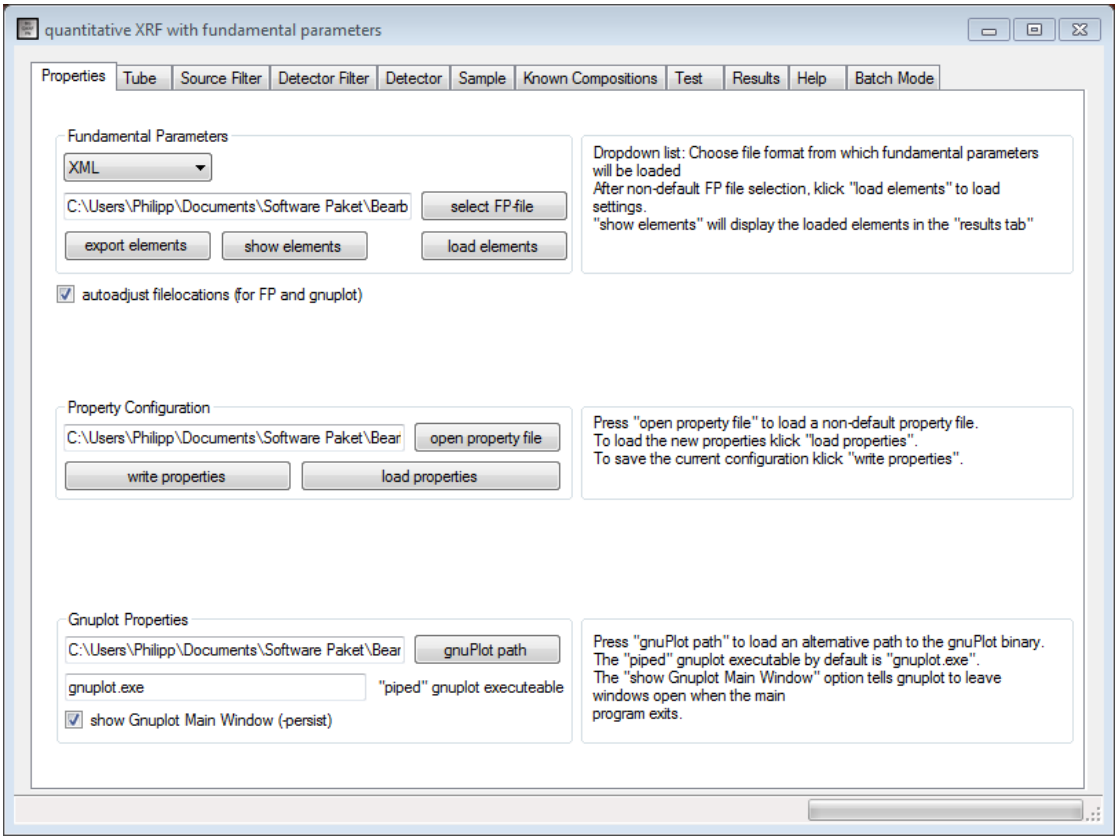

Figure 3.1.: Properties tab to manage all general settings of BGQXRFPN.

3.1.2. Property Configuration

The second category of the *Properties tab* is called *Property Configuration* and affects all settings and parameters of this software package. In this section, *property files* can be loaded and new ones can be created. These files have to be in XML file format to work correctly. A default *property file* and its possible content will be discussed later. This file is called *Properties.xml* and was also included into the software package where it can be found in the *Properties* folder.

3.1.3. Gnuplot Properties

The last category of properties are the *gnuplot properties*. It is not necessary to use the gnuplot plotting software to calculate concentrations and generate a report of a sample. If gnuplot is supposed to be used, one needs to set the binary folder of gnuplot as well as the binary name within the software or a *property file*. The checkbox *show Gnuplot Main Windows (-persist)* allows the user to select if a gnuplot window is supposed to be closed when a second gnuplot window opens. Checking the checkbox will activate the gnuplot *-persist* option, which will keep any gnuplot window. All the gnuplot settings can also be made by using an appropriate

property file after the start of the program. Deleting the gnuplot settings from a *property file* will force the program to load it's default settings while loading the modified file. If file locations whithin the BGQXRFPN software package have been changed by the user, the gnuplot integration may not work. In this case one has to manually select the path and the binary name of gnuplot (e.g. if gnuplot is already installed into another folder).

3.2. Tube

The *Tube tab* is separated into two further tabs: the *primary tube* and the *secondary target*. Settings within the secondary target will only take effect if the *use secondary target* checkbox is checked. This can also be managed with a *property file* by selecting the corresponding options.

3.2.1. Primary tube

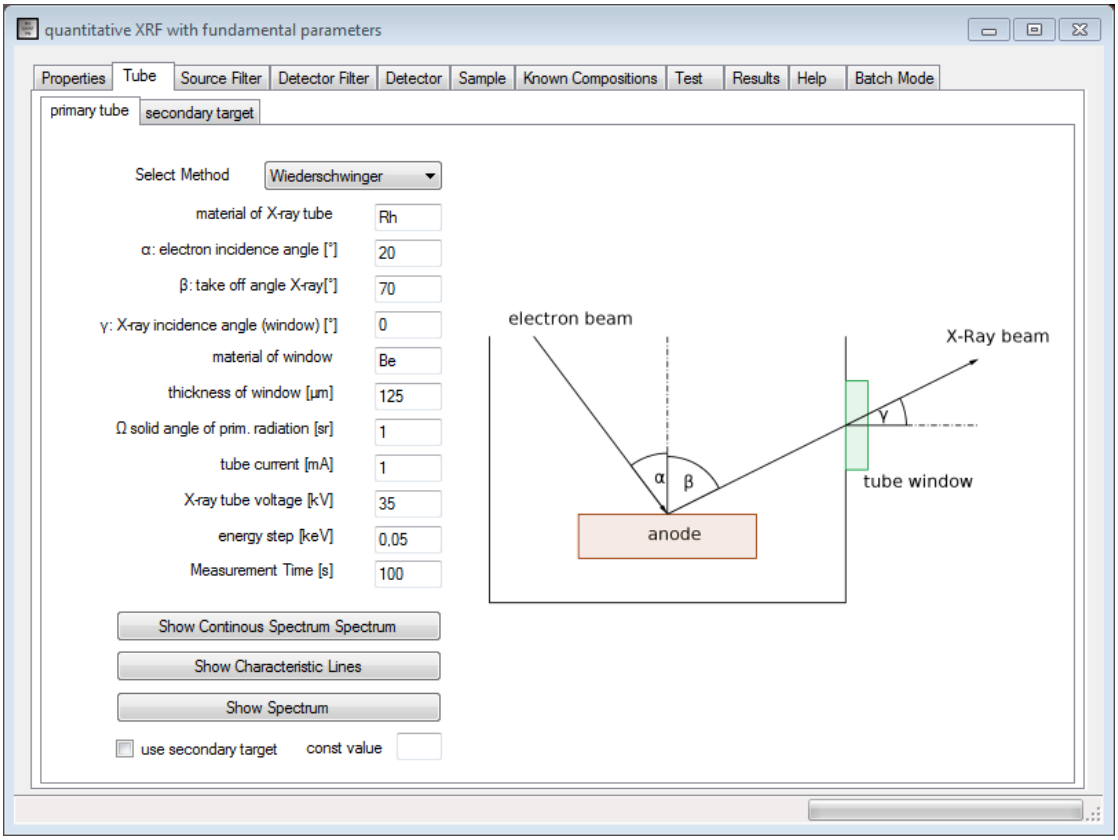

Figure 3.2.: Primary tube tab to manage the simulation of the X-ray tube.

Within the *primary tube* tab, all settings of the X-ray tube can be managed. With a dropdown menu one can select between two X-ray tube simulation methods: *Wiederschwinger* [14] and *Love & Scott* [15, 16]. The anode material as well as the window material of the tube can be any element of the peridoic system, or a composition from the *Known Compositions tab*. Note that the simulation model of the X-ray target material is only designed for pure elements.

Spectra can be displayed in three different ways. It is possible to show the *continous spectrum*, the *characteristic lines* and the whole *spectrum*.

The *use secondary target* checkbox allows the addition of a secondary target to the calculation setup.

For debugging purposes one can set the output number of photons constant for the simulation of the X-ray tube.

3.2.2. Secondary target

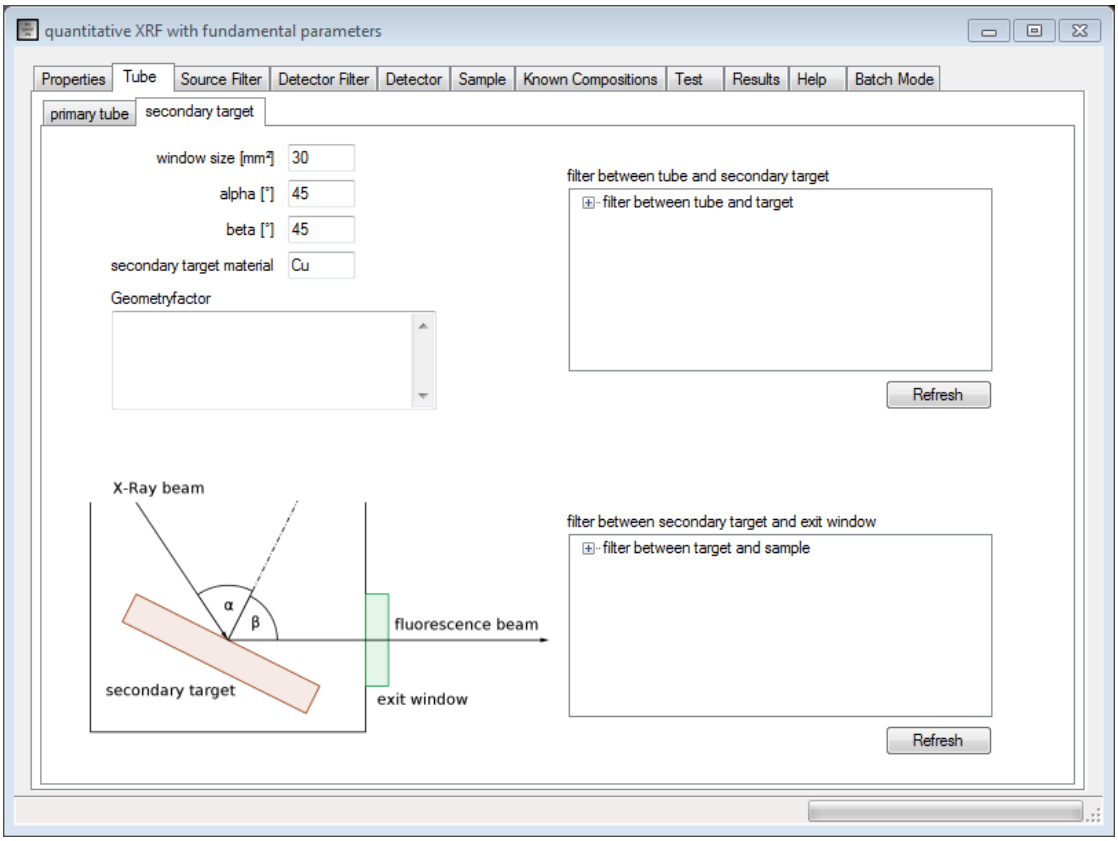

Figure 3.3.: Secondary target tab to manage the simulation of an additional secondary target.

If the *use secondary target* checkbox is selected in the *primary tube tab*, the settings in the *secondary target tab* will take effect.

It is possible to select the material of the secondary target, the window size of its exit window as well as the incident angle of the primary X-ray beam and the take off angle of the fluorescence beam. It is also possible to place multiple filters (and filterlists) between the primary tube and the secondary target and between the secondary target and the exit window. A correction factor for this setup can

also be used.

For better understanding, this tab's content has been reordered and an image of the schematic secondary target setup has been added.

3.3. Source Filter and Detector Filter

The *Source Filter tab* and the *Detector Filter* tab provide the option of adding filters to the calculation setup. *Source filters* are located between tube and sample, *detector filters* between sample and detector.

Filters can either be added manually, imported from an XML-file or directly set within an *property file*. Furthermore, it is possible to save filter settings directly to an XML-file for future calculations.

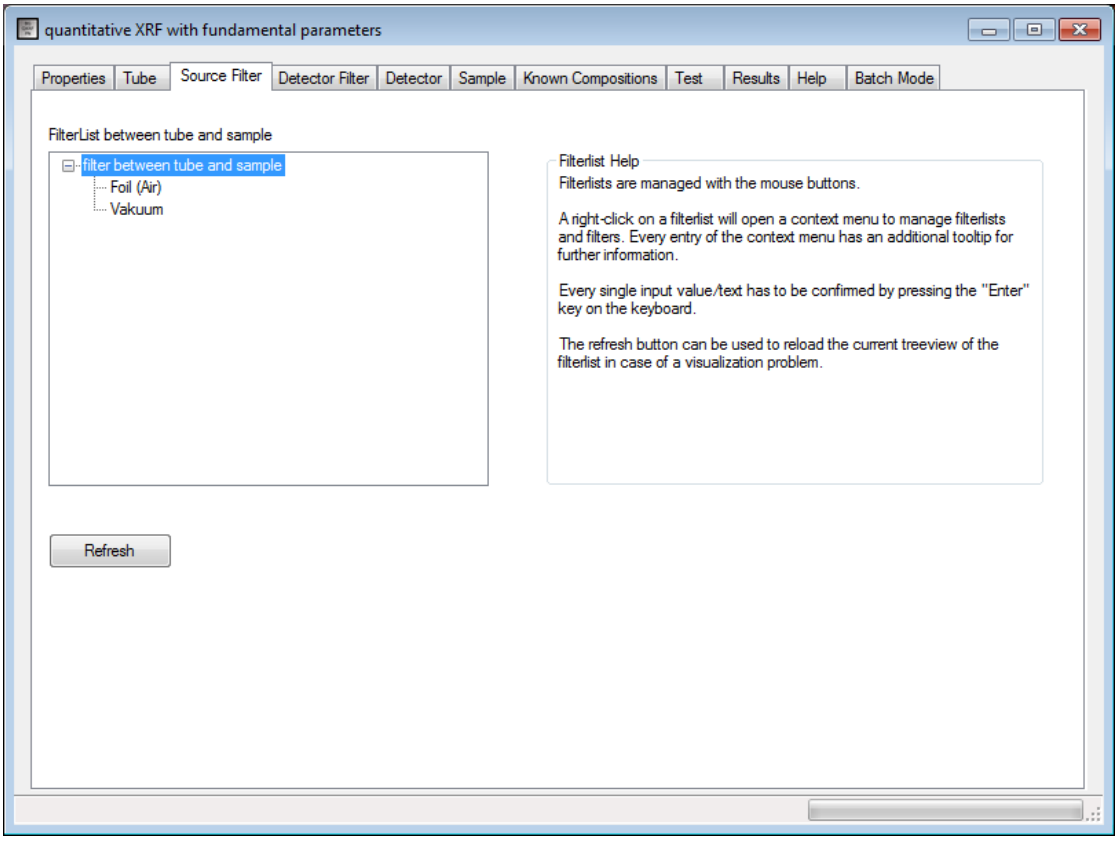

Figure 3.4.: Source filter tab to manage filters between tube and sample.

The following filters can be used inside the BGQXRFPN software package:

- Foil: Simulation of a foil filter according to the Beer-Lambert law including an enhancement factor. To use this filter, one has to set the filter material, its thickness and enhancement factor.
- Band Square: This filter is used to simulate an ideal rectangular bandpass filter. Settings include minimum energy, maximum energy and an enhancement factor.

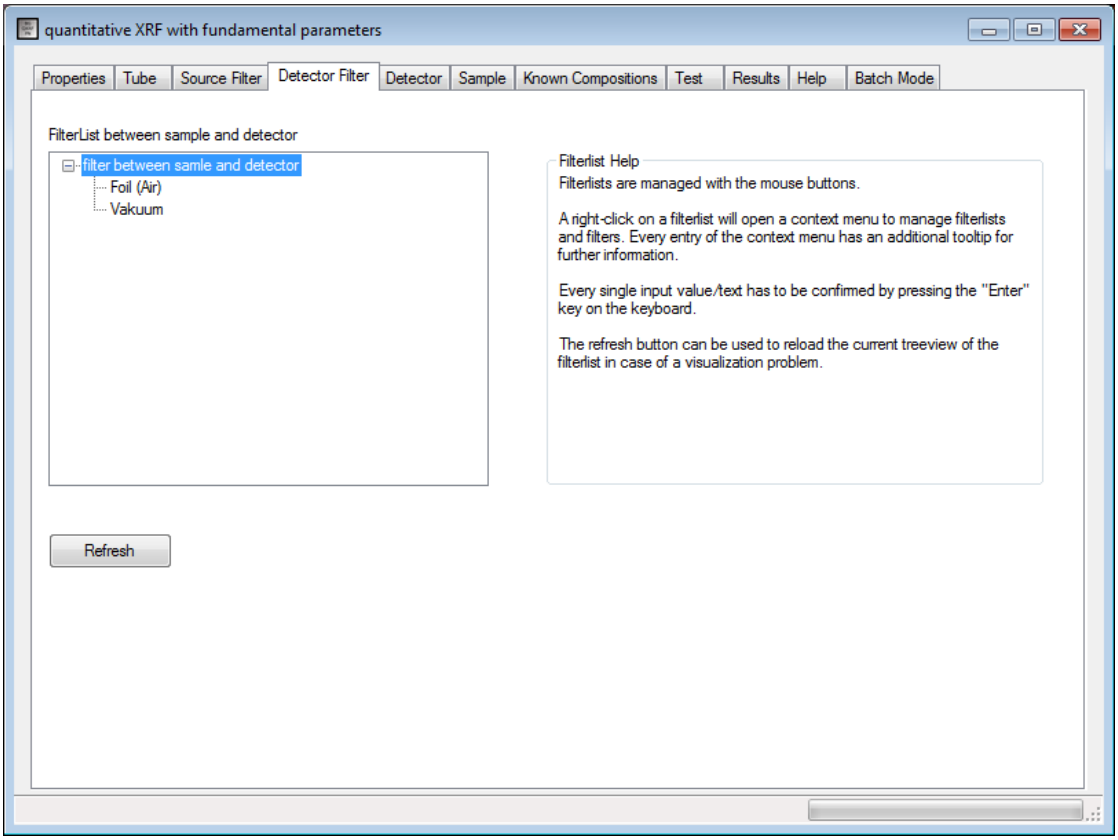

Figure 3.5.: Detector filter tab to manage filters between sample and detector.

- Gauss: The Gauss filter is used to cut out a bell-shaped curve from the spectrum. For this filter one has to set *mu* [keV] (expected value), *sigma* [keV] (standard deviation) and an enhancement factor.
- Vakuum: Among other things the vacuum filter is used to determine a geometry factor. Only thickness and its enhancement factor can be changed.
- MathFormular: The MathFormular filters can be used to calculate nearly any filter without source code changes of this software (e.g. poly capillary optics). A MathFormular filter function can be written as:

  F(E) = Y(X=E) = (enhancement factor) * (X dependend function)

  To use this filter one has to set its enhancement factor and its formular according to its scheme Y=... Eg.: Y=sin(X)+cos(X)

  Note that spaces are not allowed inside a formular.

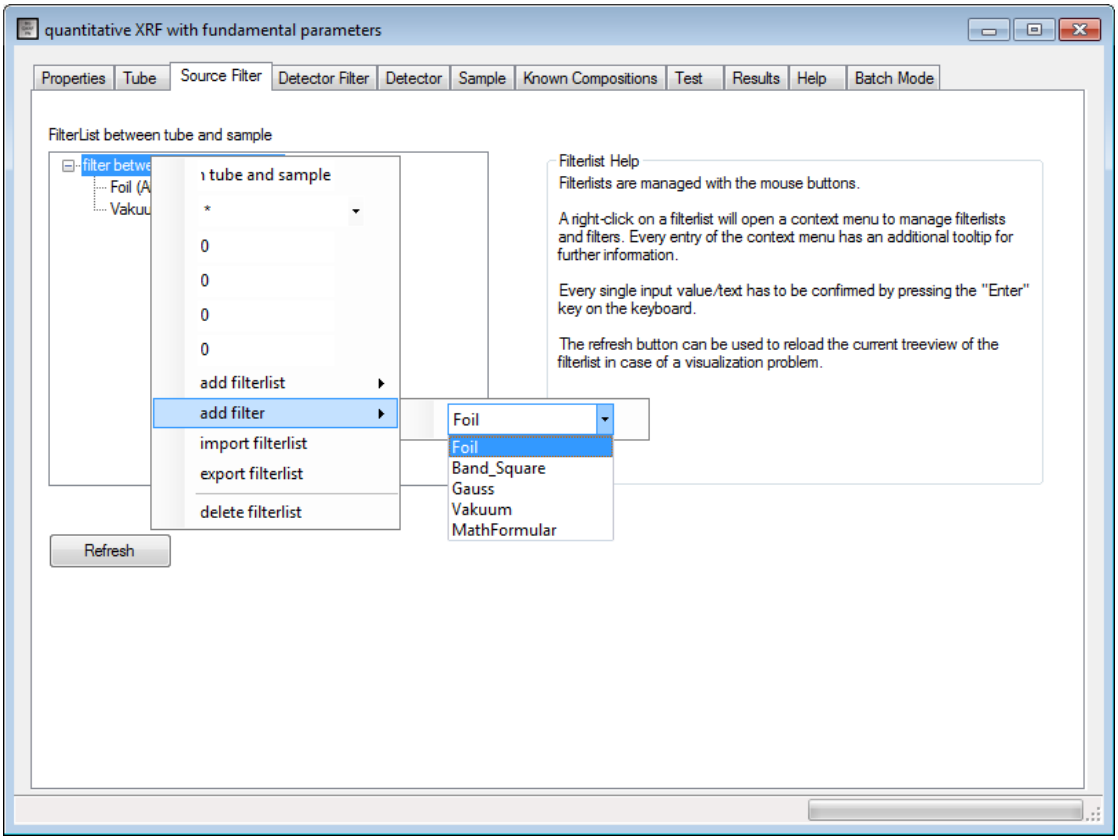

Figure 3.6.: Right-click context menu of filters showing possible filter selections.

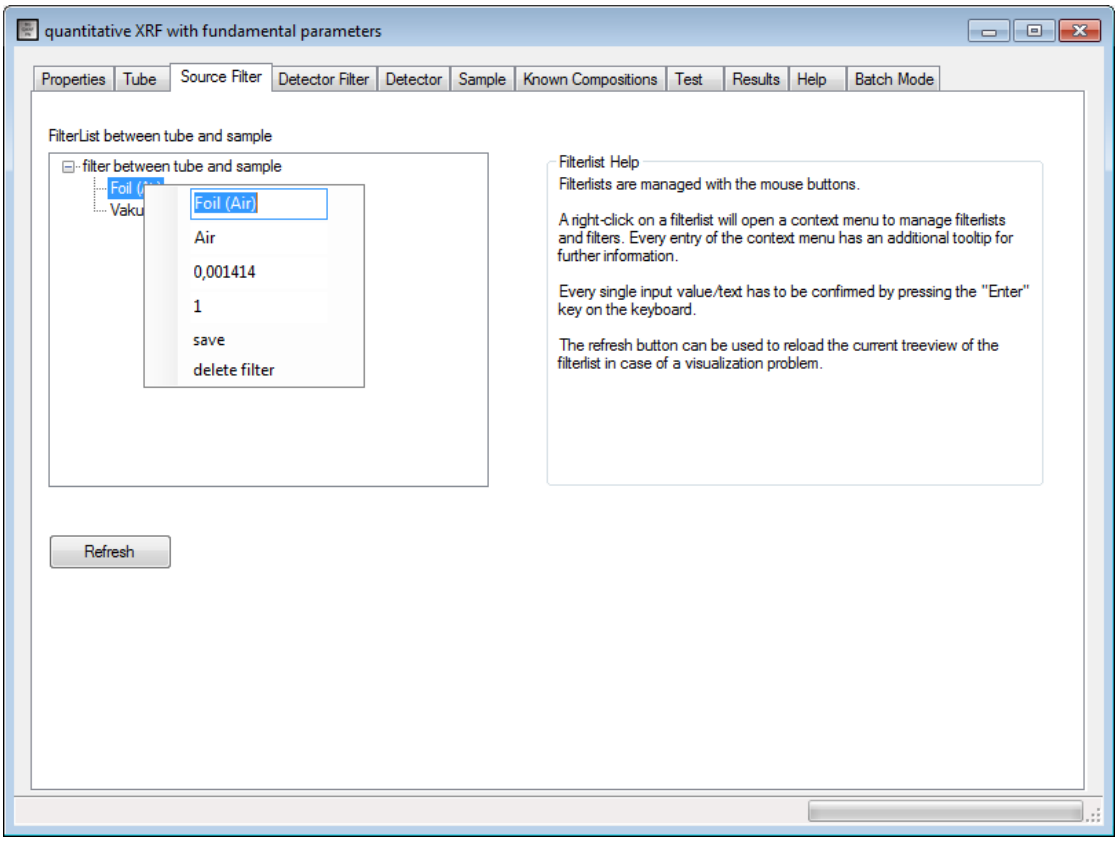

Figure 3.7.: Right-click context menu of a foil filter. The first entry represents the name of the filter, followed by the filter material, the thickness in [m], and the enhancement factor.

3.4. Detector

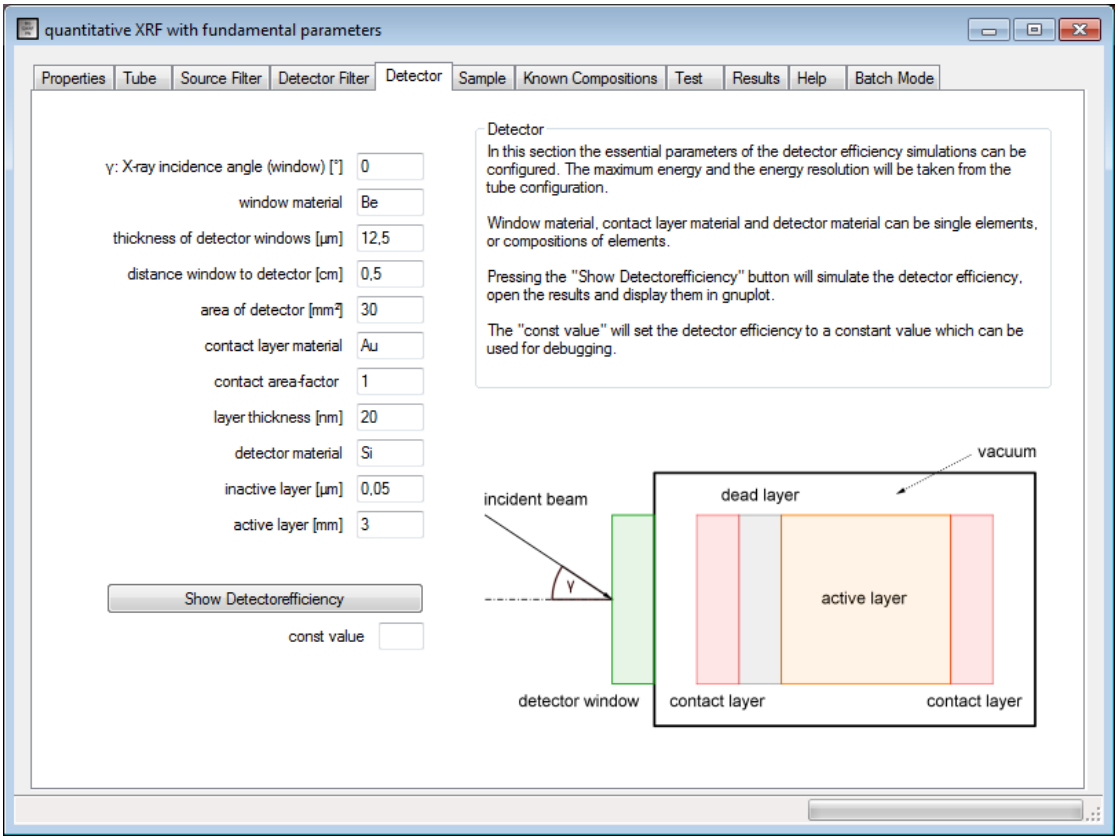

Figure 3.8.: Detector tab to manage the settings of the detector simulation.

To simulate the detector efficiency, one has to set all parameters of the detector within the *Detector tab*. Maximum energy and the energy resolution will be taken from the tube configuration. Window material, contact layer material and detector material can either be single elements or compositions of elements from the *Known Compositions tab*.

Plotting the detector efficiency with gnuplot can be realized by selecting the *Show Detectorefficiency* button. For debugging purposes the detector efficiency can also be set to a constant value.

3.5. Sample

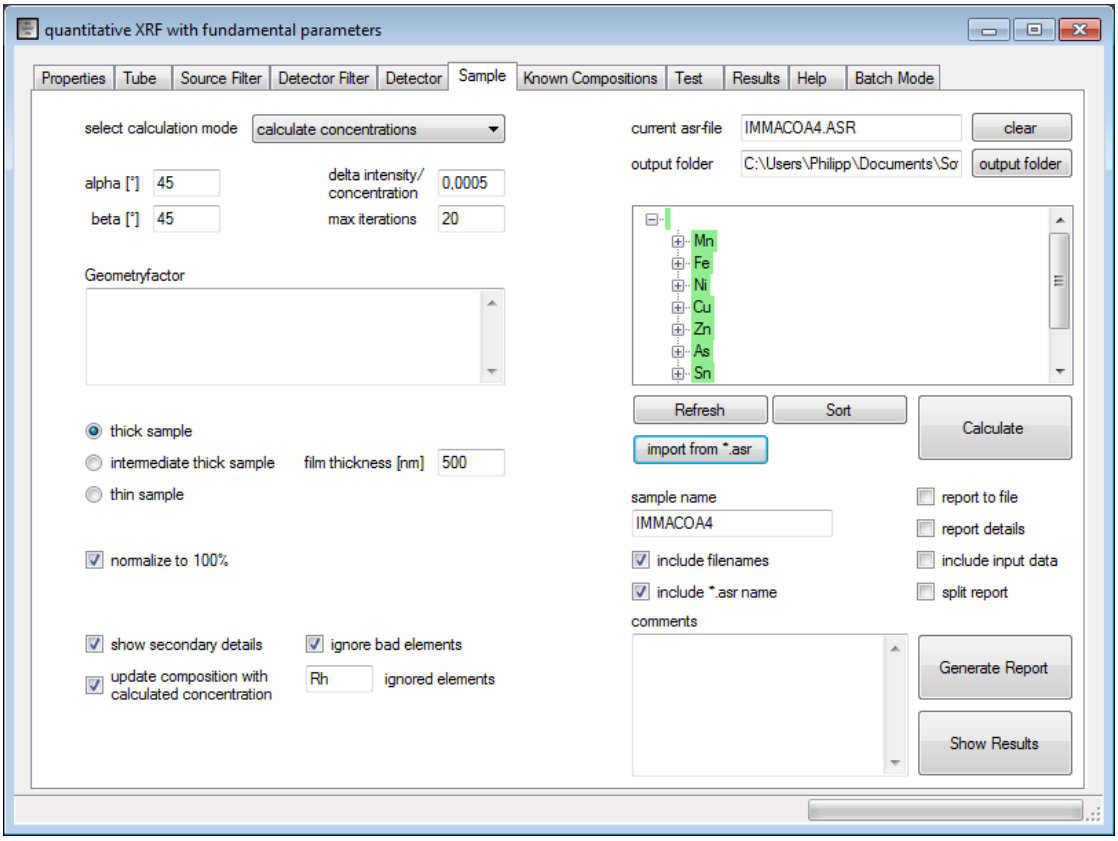

Figure 3.9.: Sample tab for sample settings, calculation settings and report settings. In this figure, a sample ASR-file has been imported to the software package.

The sample configuration and the calculation settings can be made in the *Sample tab*.

On the left side, the calculation method has to be selected. The following three methods are implemented into the software package:

- *calculate concentrations*
- *calculate intensities*
- *compare relative intensities*

After selecting the calculation method, one has to set the *delta intensity/concentration* and the *max iterations*.

The incidence angle of the primary radiation and the fluorescence beam of the

sample have to be selected according to the image in the *primary tube tab*. A correction factor can also be used if the sample is not normalized to 100%.

Three types of sample simulation models can be used:

- *thick sample*
- *intermediate thick sample*
- *thin sample*

When selecting *intermediate thick sample* or *thin sample*, one has to set the *filmthickness* in nanometers to reach the right results. The thickness of the sample does not effect the simulation of *thick samples*.

Show secondary details will show the details about which amount of intensity is induced by secondary emission. To use the calculated concentrations within the software, *update composition with calculated concentration* has to be checked. To ignore single or multiple elements during ASR-file import, one can select *ignore bad elements* and type in the desired elements into the corresponding textbox. To exclude multiple elements from the import, one has to separate each element by using a comma (e.g.: Rh,Fe,Ni,Zn).

The currently loaded ASR-file will be shown in the upper right part of the *Sample tab*. The name of the ASR-file will also be used as report filename (except for the extension change from .asr to .txt) and will be shown in the *sample name* textbox. The sample name can also be changed manually. Note that this sample name textbox will not change the name of the report filename, but the name of the sample within the report. The report filename can be changed after selecting *report to file* and generating the report. The output folder for the generated reports can be selected by using the *output folder* button.

If display errors occur after an ASR-file import or calculation of a sample, the *Refresh* button will reload the sample window. To sort a sample according to the atomic numbers of its elements, one can use the *Sort* button.

To include the filenames and locations of the *fundamental parameters* file and the *property file* to the report, one has to check the include filenames checkbox. The ASR-filename and its path can be added by selecting *include *.asr filename*.

After setting all the parameters, the calculation of the sample can be started with the *Calculate* button. The progress will be shown in the status bar.

To generate a report after the calculation one can select:

- *report to file*: to write the report to a TXT-file

- *report details*: to include transition energy, edge energy, calculated relative intensity, measured absolute intensity, calculated absolute intensity and relative intensity
- *include input data*: to include imported or manually set parameters of the sample (e.g. intensities)
- *split report*: to split the report into a results and an input file. This only takes effect if *report to file* and *include input data* are selected.

In addition it is possible to use a specific *sample name* and add *comments* to the report. As mentioned before, the ASR-filename of an imported file will be taken as the default *sample name*. If no file import was done, this textbox will be left empty by the BGQXRFPN software package.

The report itself will be generated after clicking the *Generate Report* button. A file dialog will open to select filename and file path. To show the results of the calculation within BGQXRFPN, select the *Show Results* button to switch to the *Results tab*.

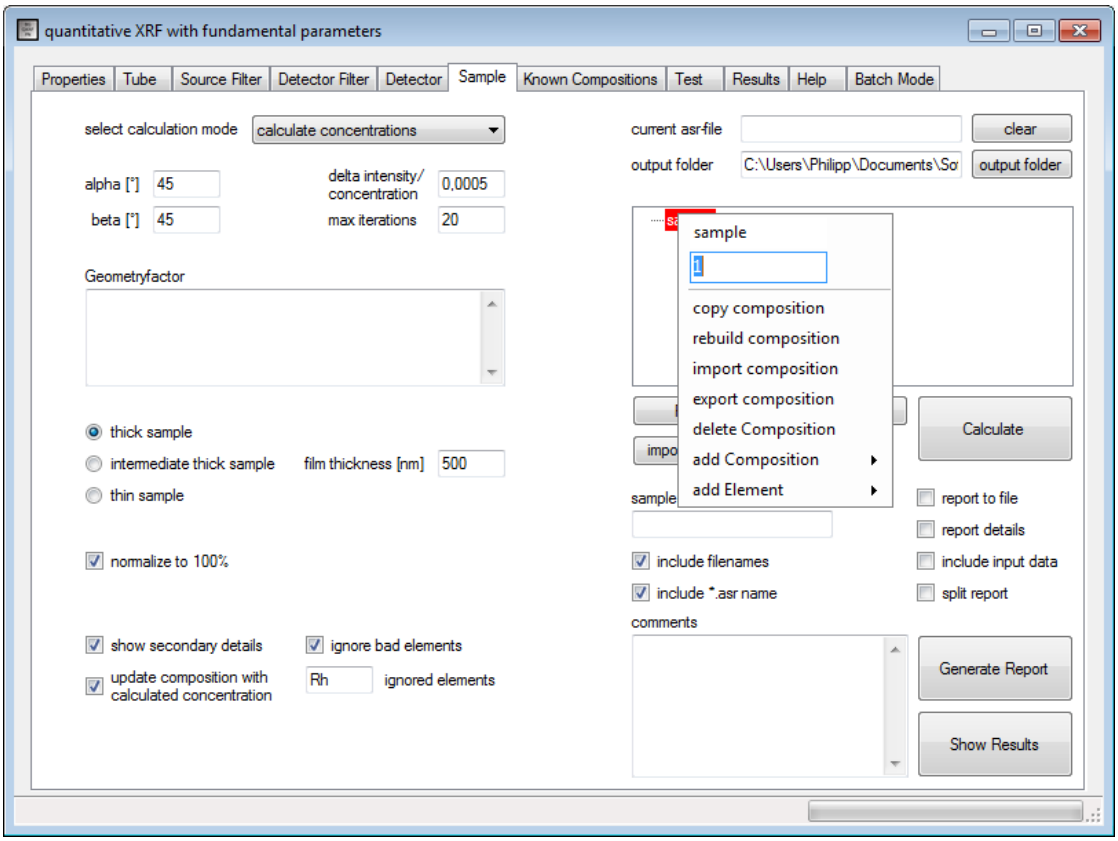

Figure 3.10.: Right-click context menu of the sample tab showing manual sample selection.

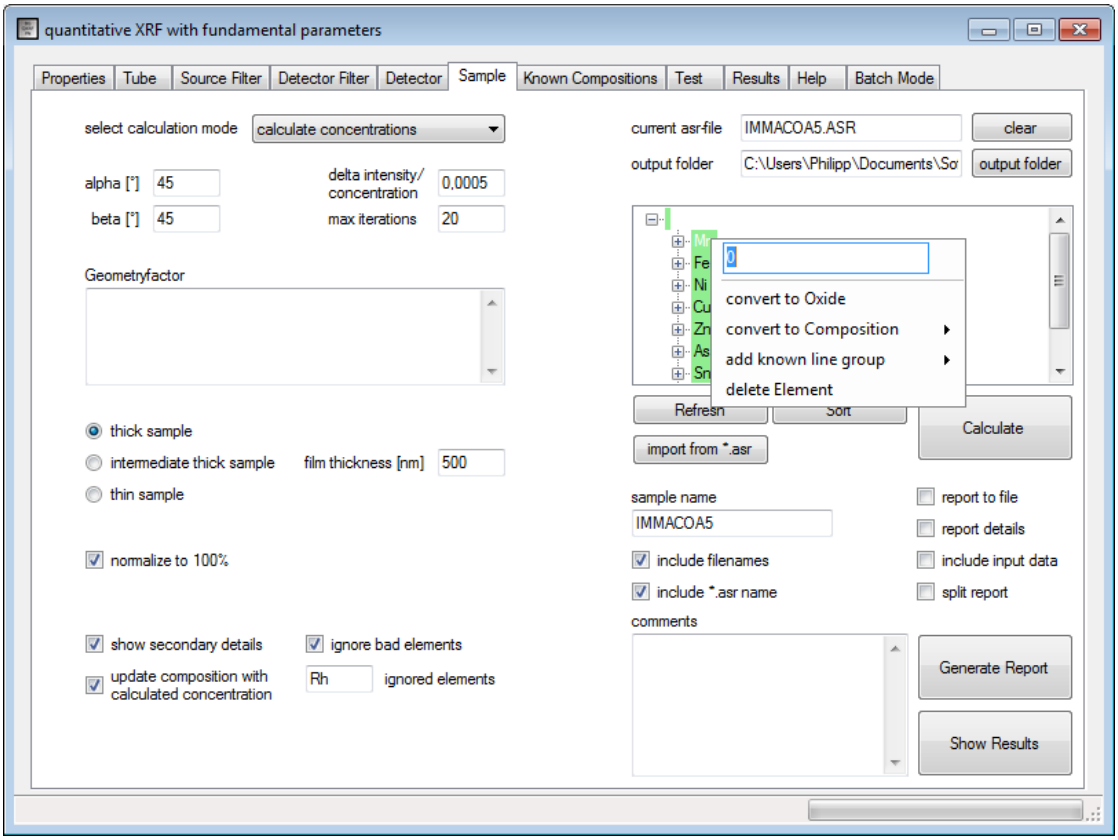

Figure 3.11.: Content of the right-click context menu from the sample tab while selecting an imported element from an ASR-file.

3.5.1. Quick guide to calculate a single sample

1. Launch BGQXRFPN
2. Load a *property file* or set the parameters of tube, filters and detector manually
3. Switch to the *Sample tab* and set the sample and calculation parameters
4. Import an ASR-file by clicking the *import from *.asr* button
5. Check the sample for any errors
6. Start the calculation by selecting the *Calculate* button
7. Generate a report by selecting the desired settings and click *Generate Report*

3.6. Known compositions

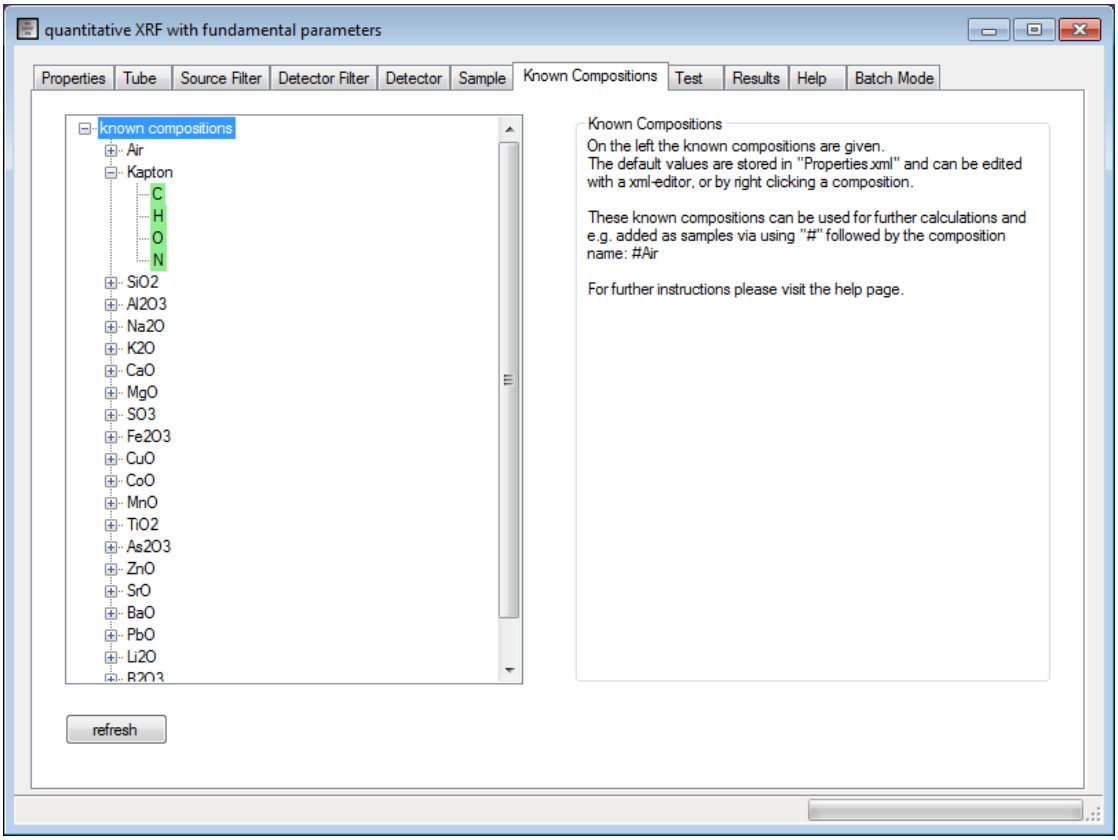

Figure 3.12.: *Known Compositions tab* to handle and access the known compositions within the software package.

Within the *Known Compositions* tab, known compositions of elements can be included into the software package. They can be managed manually, imported from a *property file*, or imported from an XML-file using the right-click context menu. These known compositions can for example be used as target material, window material or as samples by accessing them by their name. Elements of a sample that are to be changed into an oxide will be converted according to the known compositions. It is also possible to convert elements into compositions which are content of the known compositions (Fig. 3.13).

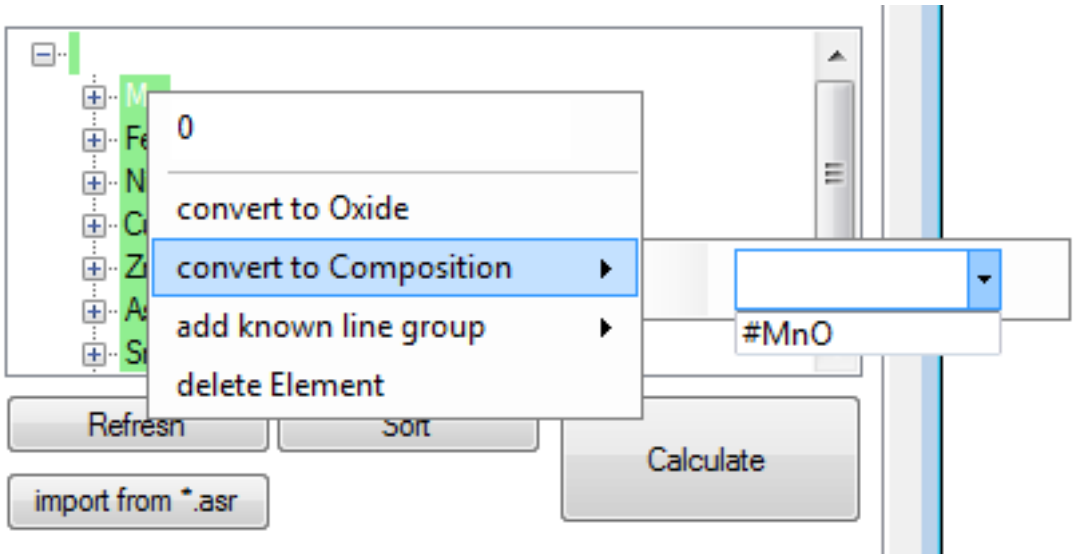

Figure 3.13.: Right-click context menu to convert an element to a known composition. Here Mn was selected to be converted into a composition from the *known compositions*, where MnO is included.

3.7. Test

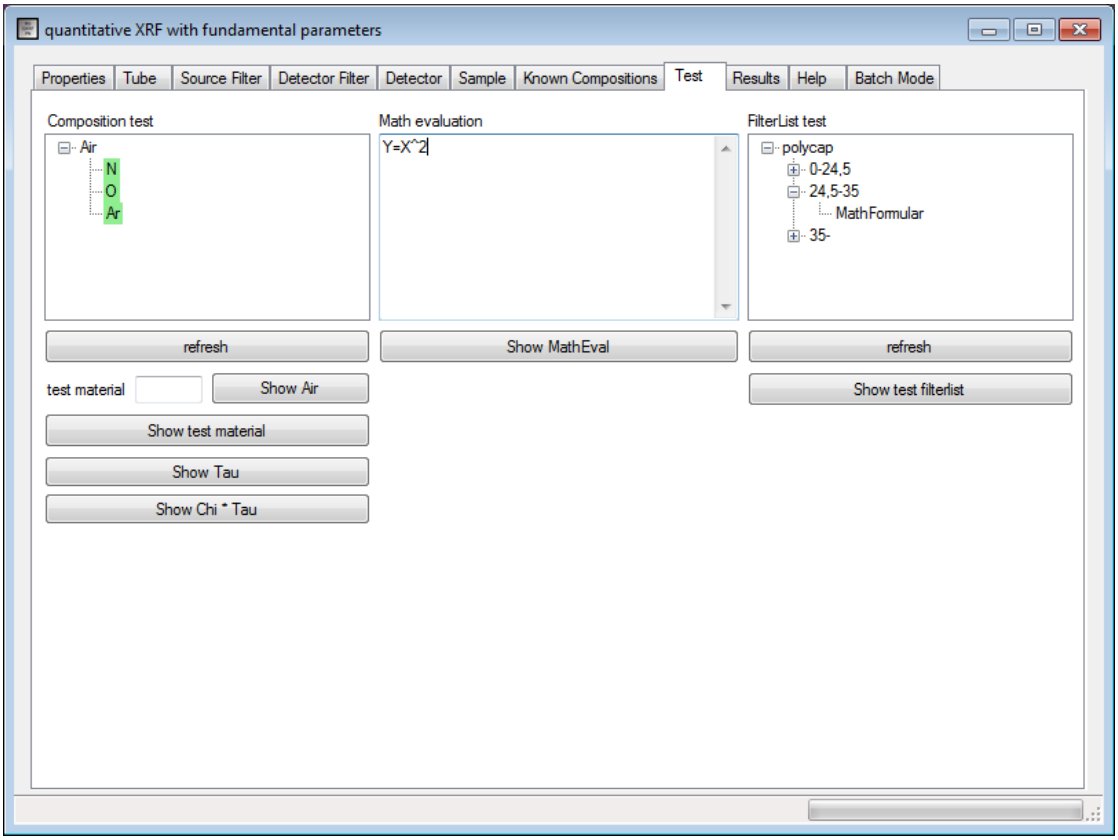

Figure 3.14.: Test tab for debugging and simulation purposes. It is possible to simulate samples, correction functions as well as filters and filterlists.

The *Test tab* appears in a new design with three columns. Each column handles a different task to test the different properties and settings of the software.

3.7.1. Testing compositions

Testing of compositions is possible either after the manual creation of samples with the right-click context menu, or after the import of samples from an XML-file. The *Refresh* button will reload the tree view of the sample in case of display errors. Selecting a composition from the *Known Compositions tab* without using the context menu can be done by setting compositions with the *test material* textbox and confirming with the enter key. The *Show test material* button will open the *Results tab* of BGQXRF and show the composition of the sample.

The *Show Tau* button will open gnuplot and plot the mass absorption coefficients ($\mu, \tau, \sigma_{coh}, \sigma_{inc}$). It will print them in the *Results tab* where they can also be saved as a file.

3.7.2. Testing the mathematical parser

Correction factors and mathematical filters can be tested with the *Math evaluation* section. A plot of the edited function can be created by selecting the *Show MathEval* button.

The format of the mathematical function can be for example:

- Y=(100*pi)/(18*(X^2))
- Y(X)=A*cos(X)+B*sin(X)
  A=exp(X)
  B=tanh(10)
- Y=4*pi*(10^(-12))

3.7.3. Testing filters and filterlists

Testing filters and filterlists which were manually created or imported from an XML-file can be done in the *FilterList test* section. Already tested mathematical functions for e.g. polycap filters can be used in mathematical filters. Energy and absorption can be displayed with gnuplot by clicking the *Show test filterlist* button. In case display errors within the *FilterList test* section occur, the content can be reloaded with the refresh button.

3.8. Results

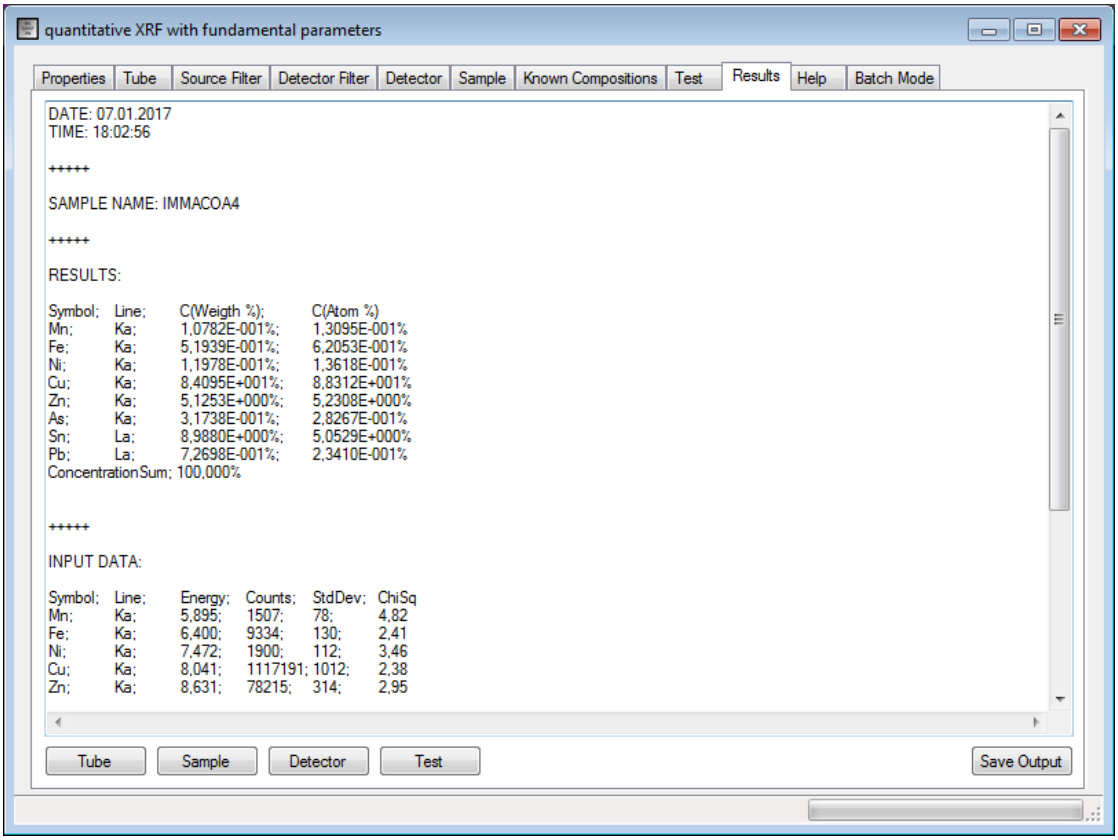

Figure 3.15.: Results tab to access the output of the software package.

To access the output of the software package, the *Results tab* has been created. All calculation or testing output will be shown inside its textbox. The output can either be saved by clicking the *save results* button, or by selecting and copying the output text directly from the textbox. The default output file format is TXT. Copied text can easily be imported to software like *Microsoft Excel* for further use.

For better navigation in the BGQXRFPN software, quick-buttons to change tabs are positioned at the bottom of the output textbox.

3.9. Help

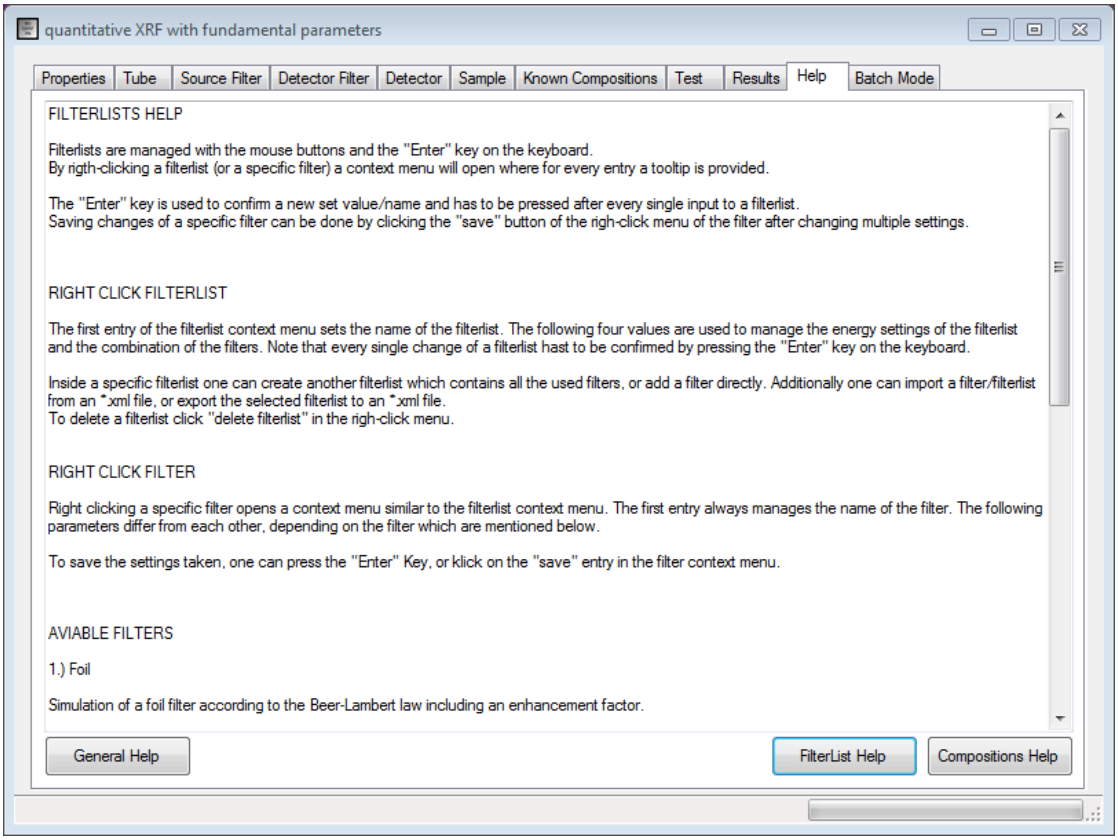

Figure 3.16.: Help tab to obtain further information about BGQXRFPN.

A short documentation of BGQXRFPN can be accessed by the *Help tab*. It is divided into three parts which can be accessed by its buttons:

- General help
- Compositions help
- FilterLists help

Selecting one of the three help pages changes the content of the main window to the selected help page.

The *General Help* gives a short overview about every setting which can be made by the user. It is not a full documentation of the BGQXRFPN software package. A short introduction about filters and filterlists within this software can be accessed by clicking the *FilterList Help* button. Further information about the use of compositions can be obtained in the *compositions help*.

3.10. Batch mode

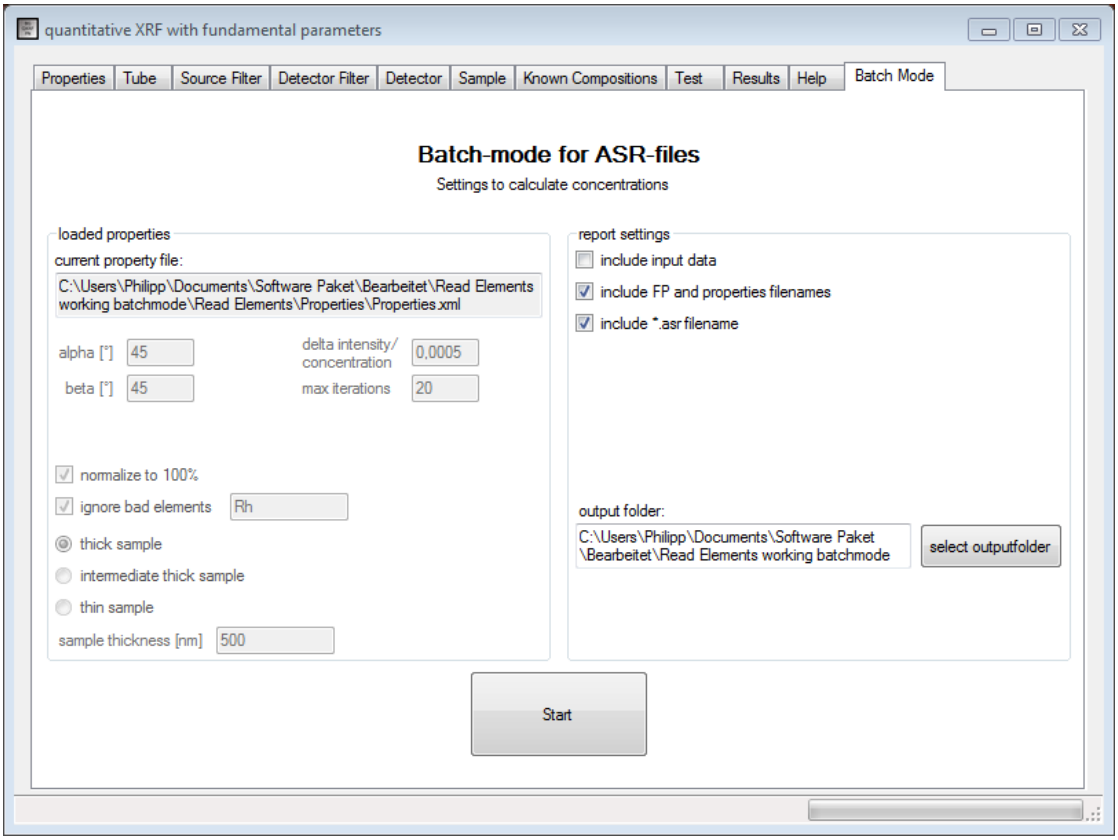

Figure 3.17.: Batch mode of BGQXRFPN.

The *batch mode* was designed completely from scratch to calculate concentrations of ASR-file input data. It is divided into two columns: the *loaded properties* on the left side and the *report settings* on the right side.

The left column is not editable by the user. It lists all the settings made or loaded within the software. The *batch mode* is intended to be used with a preconfigured *property file*. The currently loaded file will be shown in a gray textbox. All settings will be taken from the property file and can be changed manually within the program.

In the right column, the settings for reports generated by the *batch mode* can be selected. It is possible to include the input data from each corresponding ASR-file. Moreover the file locations of the used fundamental parameters file, the property file, and the ASR-file can be selected to be included into the report. Before the calculation, one can select an output folder where the report files will be stored. When selecting the *Start* button, a file dialog window will open to choose multiple

ASR-files for calculation. To select all files in a folder, hit *Ctrl + A* on the keyboard. To select multiple files in a row, keep holding the *shift* key while selecting the first and the last file of the row. If multiple files in a folder shall be selected and they are not in a row, one has to keep holding the *Ctrl* key and select the files with the mouse.

3.10.1. A quick guide to use the batch mode

1. Create or select a proper *property file* and load the properties
2. Set tube, filter, sample and detector settings if they are not already configured inside the *property file*
3. Switch to the *Batch Mode tab* and check settings in the left column
4. Set report settings and output folder
5. Click the *Start* button to select the files to calculate and begin the actual calculation
6. When the calculation is done, a message box will appear and inform the user. The report files will be located in the selected output folder.

4. Property files

A *property file* (e.g. *Properties.xml*) is one of the two XML input files wich will be loaded at program start. It is used to set all parameters of the software, the measurement setup (including tube, filters and detector), and the sample properties. *Property files* can also be used to calculate multiple ASR-files automatically with a given setup in the batch mode. Default *property files* are provided in the BGQXRFPN software package for different setups.

Note that it is not necessary to provide a *property file* at program start. It can be selected afterwards, or alternatively the default values of BGQXRFPN can be used. If an error occurs or the *property file* is missing, a message box with a warning will be shown.

The Properties.xml files can be created and managed in two different ways:

1. with the BGQXRFPN software package
2. with an XML-editor

Within this chapter, both ways will be discussed after an introduction about the settings and properties within a Properties.xml file.

4.1. Components of a property file

A Properties.xml file is generally divided into 5 sections:

1. general settings
2. calculation settings
3. report settings
4. tube, filter, sample and detector settings
5. known compositions settings

Each one of this sections can contain boolean values, strings, integer and float values. See table 4.1 for further information.

The *general settings* contain amongst others the file path of the *fundamental parameters file*, the gnuplot file path, and the gnuplot binary name. One can also

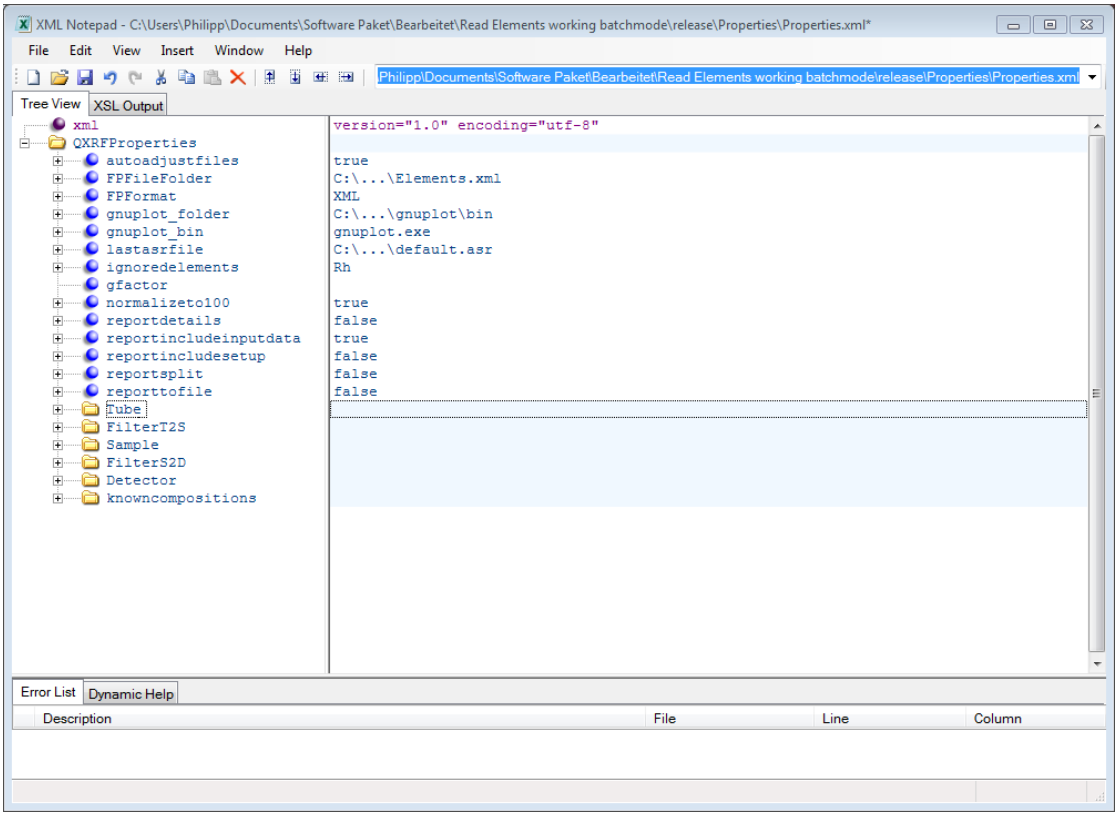

Figure 4.1.: Example of a *property file* called *Properties.xml* displayed in *XML Notepad 2007*.

choose that these settings shall be checked at the start of the program by using *autoadjustfiles*.

Calculation settings handle the sample calculation properties. For example, if a single element (or multiple) shall be ignored during ASR-file import, one can use the *ignoredelements* entry and enter the element name (e.g. Fe,Ni,Mn).

Within *report settings*, boolean values handle the content of a report which can be created after a sample calculation. Typical settings can be *reportincludeinputdata*, or *reporttofile*. While using the *batch mode* of BGQXRFPN, recommended settings are:

- *reporttofile: true*
- *reportdetails: false*
- *includesetup: false*
- *includeinputdata: true*

- *reportsplit: false*

For further information about the impacts of each report value see Tab. 4.1.

The *tube, filter, sample and detector settings* (Figs. 4.2, 4.3 and 4.5) contain all properties of the tube, sample and detector as well as all filter properties (*filter between tube and sample* and *filter between sample and detector*). Tab. 4.2 discusses the detailed properties of a tube, Tab. 4.3 displays the content of the sample settings and its calculation properties. The detector settings and properties are discussed in Tab. 4.4 and the use of filters within a *property file* is discussed in an example with a foil filter in Tab. 4.5.

Note that filter settings will probably contain unused and unusable features (displayed in Tab. 4.5) due to the generation of *property files* within the BGQXRFPN software package. Bold written entries do not contain values, but are part of the internal structure. It is highly recommended to create specific filters with BGQXRFPN and either write them directly into a *property file*, or save the filter settings to an XML-file using the right-click context menu of the filter tabs.

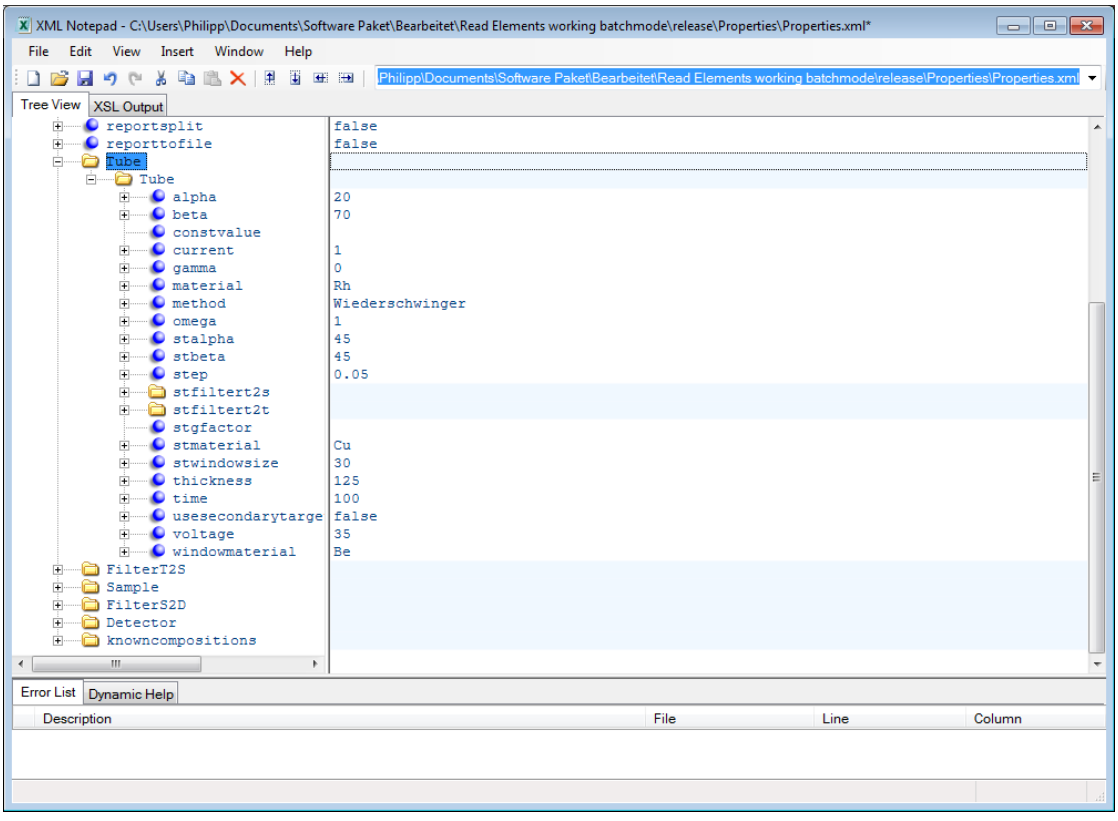

Figure 4.2.: Example of the *tube* section of a *property file* in *XML Notepad 2007*.

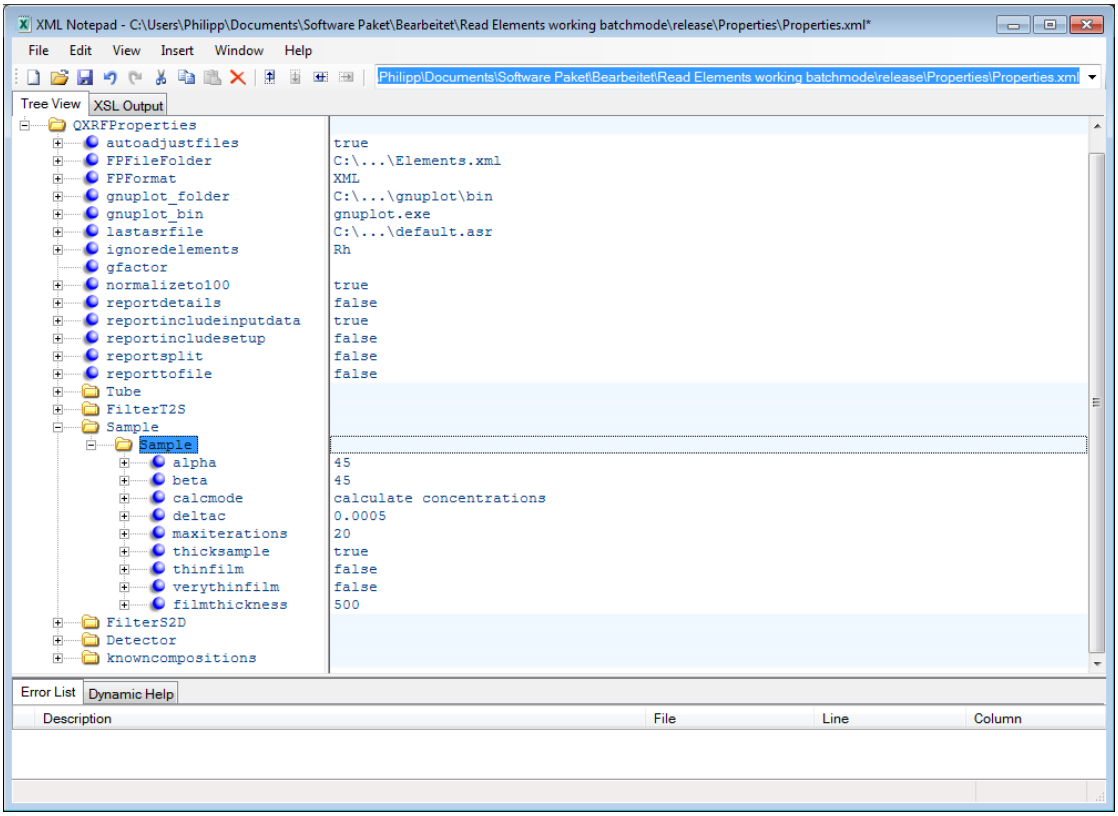

Figure 4.3.: Example of the *sample* section of a *property file* in *XML Notepad 2007*.

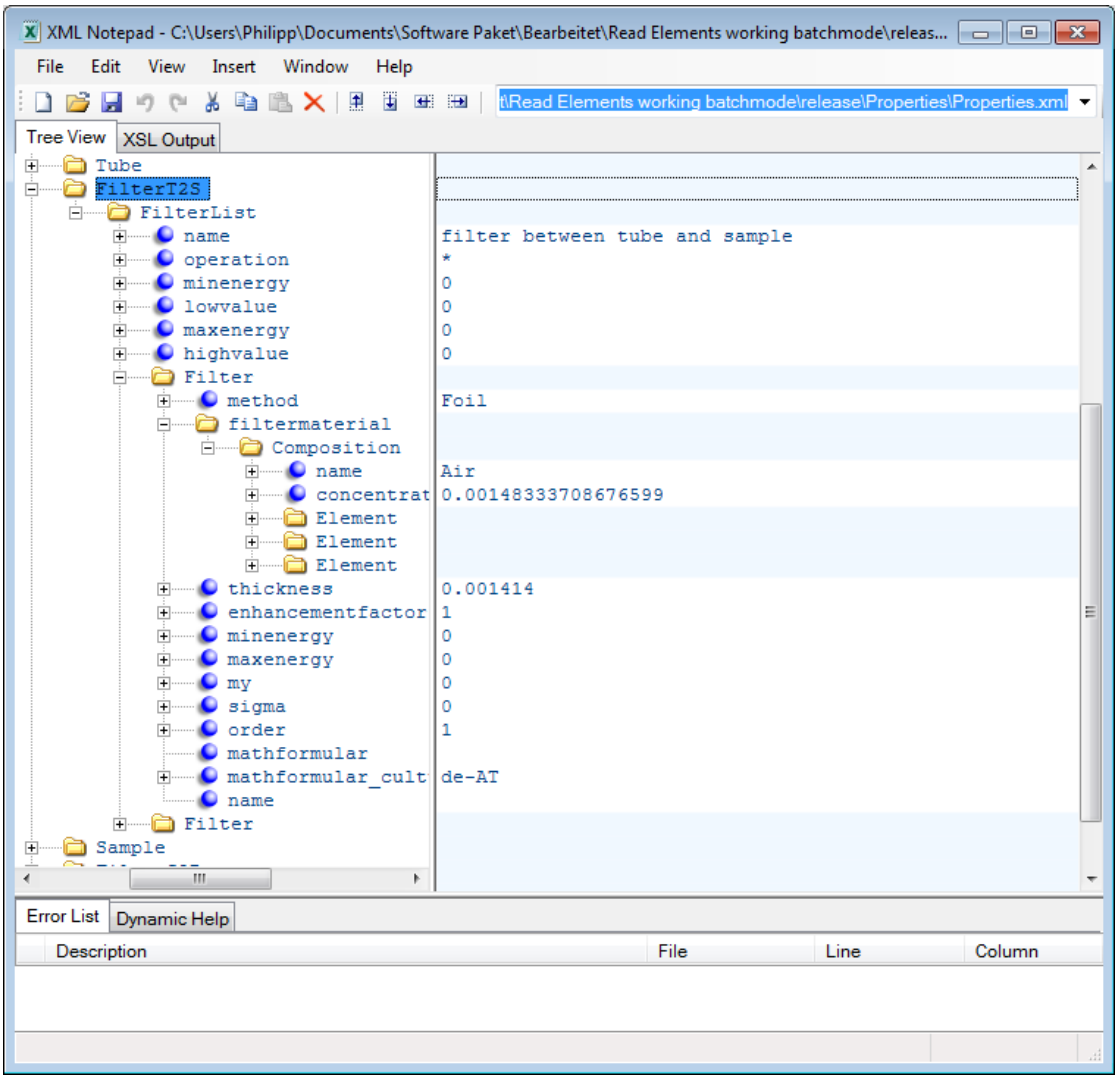

Figure 4.4.: Example of a foil filter configuration within a *property file*.

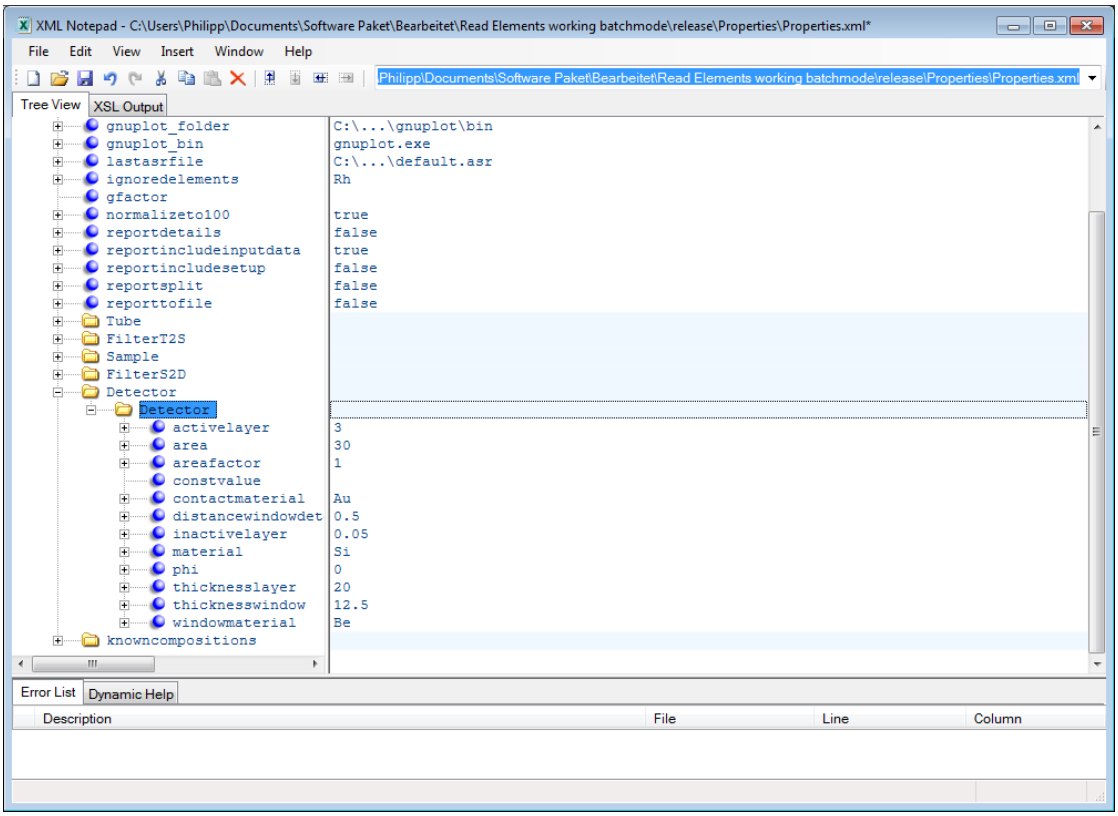

Figure 4.5.: Example of the *detector* section of a *property file* in *XML Notepad 2007*.

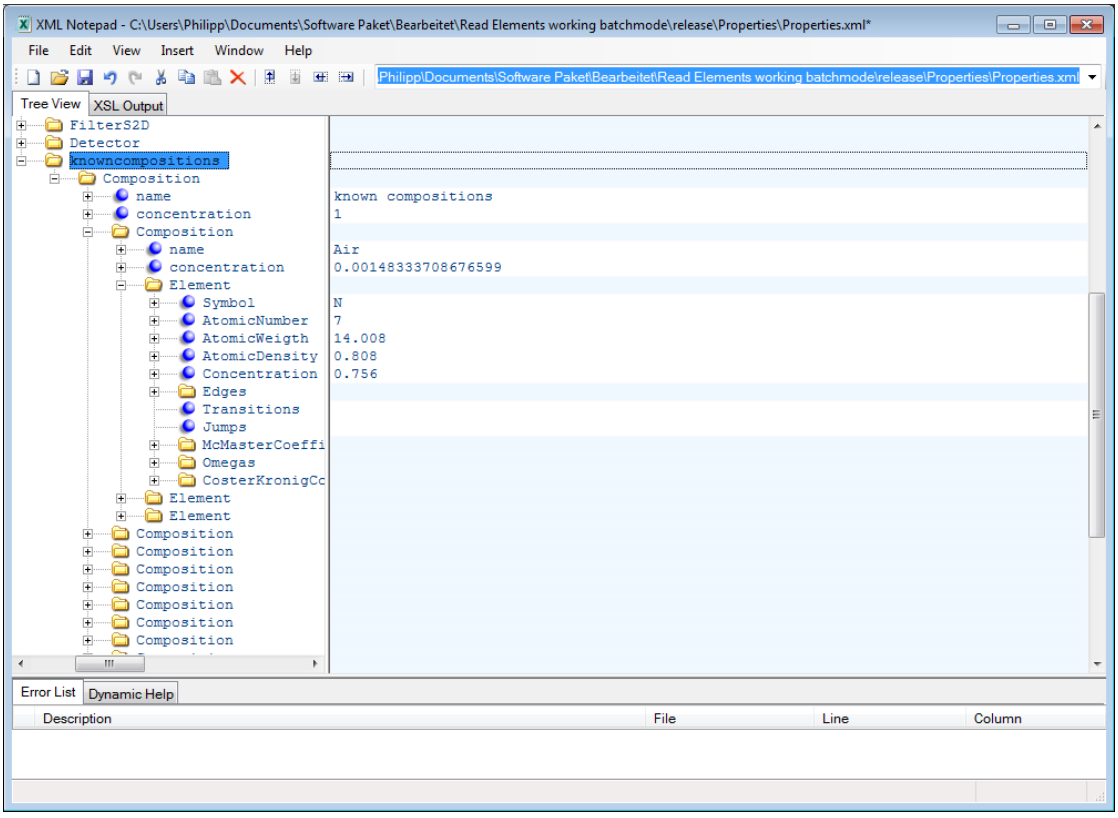

Figure 4.6.: Example of the *known compositions* section of a *property file* in *XML Notepad 2007*.

All the known compositions of elements are stored within the *known compositions settings* at the start of the program (Fig. 4.6). If another *property file* is loaded, the previous *known compositions* will be overwritten with those inside the loaded file. It is not necessary to include *known compositions* to a *properties file*, because it is possible to load them manually inside the *known compositions tab* of the program from an XML file. The content of such an XML file can be created with the right-click context menu of the *Known Compositions tab* and can be added manually to any *property file*.

General settings	
autoadjustfiles	true/false - do/don't check file locations at program start
FPFileFolder	path to fundamental parameters file (Elements.xml)
FPFormat	XML/Ebel/Darek
gnuplot_folder	path to gnuplot binary folder
gnuplot_bin	gnuplot binary name
lastasrfile	path to a single ASR-file, which will set the default opening path of the ASR-filedialog
Calculation settings	
ignoredelements	contains a string to skip the import of a single or multiple elements from an *.asr file (e.g. Rh,Fe,Cu to skip Rhodium, Iron and Cupper)
gfactor	correction factor which has to be taken into account if the sample is not normalized to 100%
normalizeto100	true/false - normalize sample to 100% (no *gfactor* needed)/don't normalize sample
Report settings	
reportdetails	true/false - do/don't include details to report
reportincludeinputdata	true/false - do/don't include information from *.asr file in the report
reportincludesetup	include the setup in the report
reportsplit	true/false - split/don't split report into input data and output data (together with *reporttofile*)
reporttofile	true/false
Tube, filter and detector settings	
Tube	contains all tube properties
FilterT2S	contains filterlists and filter settings which are located between tube and sample
Sample	contains all sample settings
FilterS2D	contains filterlists and filter settings wich are located between sample and detector
Detector	contains all detector properties
Known compositions settings	
knowncompositions	this section contains all the *known compositions*

Table 4.1.: Possible content of a Properties.xml file. Bold entries contain further options which are discussed in tables 4.2, 4.3 and 4.4.

Tube, filter and detector settings	
method	simulation method
material	material of X-ray tube
alpha	electron incident angle [°]
beta	take off angle X-ray [°]
gamma	X-Ray incidence angle (window) [°]
windowmaterial	window material
thickness	window thickness [μm]
omega	solid angle of primary radiation [sr]
current	tube current [mA]
voltage	X-ray tube voltage [kV]
step	energy step [keV]
time	measurement time [s]
constvalue	set output to a constant value of photons
usesecondarytarget	true/false
stmaterial	secondary target material
stalpha	secondary target incident angle [°]
stbeta	secondary target take off angle [°]
stfiltert2t	secondary target filter between tube and target
stfiltert2s	secondary target filter between target and sample
stgfactor	secondary target correction factor
stwindowsize	secondary target window size [mm^2]

Table 4.2.: Detailed content of the *tube* section of a Properties.xml file.

Sample settings	
alpha	incident angle of the primary beam
beta	exit angle of the fluorescence beam
calcmethod	calculate concentrations / calculate intensities / compare relative intensities
deltac	threshold value of the iterative calculation of concentrations
maxiterations	maximum amount of iteration steps
thicksample	true/false
thinfilm	true/false
verythinfilm	true/false
filmthickness	sample thickness has to be set in [nm] if the selected sample type is either thinfilm or verythinfilm

Table 4.3.: Detailed content of the *sample* section of a Properties.xml file.

Detector settings	
activelayer	active layer size [mm]
area	area of detector [mm^2]
areafactor	contact area factor
constvalue	set detector efficiency to a constant value
contactmaterial	contact layer material
distancewindowdetector	distance between window and detector [cm]
inactivelayer	inactive layer size [μm]
material	detector material
phi	X-ray incidence angle [°]
thicknesslayer	layer thickness [nm]
thicknesswindow	detector window thickness [μm]
windowmatieral	element symbol of detector window material

Table 4.4.: Detailed content of the *detector* section of a Properties.xml file.

Filter settings	
FilterT2S	location of the filter
FilterList	filters are set inside a filterlist environment
name	”filter between tube and sample” - name of the filterlist
operation	”*” - linkage type of multiple filters - selection between additive (”+”) and mutiplicative (”*”)
minenergy	(no use in foil filter)
lowvalue	(no use in foil filter)
maxenergy	(no use in foil filter)
highvalue	(no use in foil filter)
Filter	filter inside the filterlist
method	Foil
filtermaterial	settings of the filter material consisting of elements and/or compositions - should not be edited by the user to prevent errors
thickness	filter thickness in [m]
enhancementfactor	1 - do not enhance filter factor
minenergy	(no use in foil filter)
maxenergy	(no use in foil filter)
my	(no use in foil filter)
sigma	(no use in foil filter)
order	(no use in foil filter)
mathformular	(no use in foil filter)
mathformular_culture	(no use in foil filter)
name	optional filter name

Table 4.5.: Possible content of the filter settings of a Properties.xml file according to Fig. 4.4. In this example an air foil filter is discussed. Note that not every root element and value hast to be set due to the generation of *property files* within the BGQXRFPN software package. Bold written elements don't have a corresponding value to set and unused elements can be deleted.

4.2. Editing within the BGQXRFPN Software

The easiest way to save a set of properties to a specific *.xml file is to handle all settings through the BGQXRFPN software. Every change will be stored to a chosen file after clicking the *write properties* button on the *properties tab* of BGQXRFPN (Fig. 4.7). Note that the amount of settings within the software is limited.

The default filename of a property file is *Properties.xml*. If the selected filename is already taken, a consecutive numbering will be added to the name (*Properies_1.xml*, *Properties_2.xml*,...). It is also possible to overwrite a selected file.

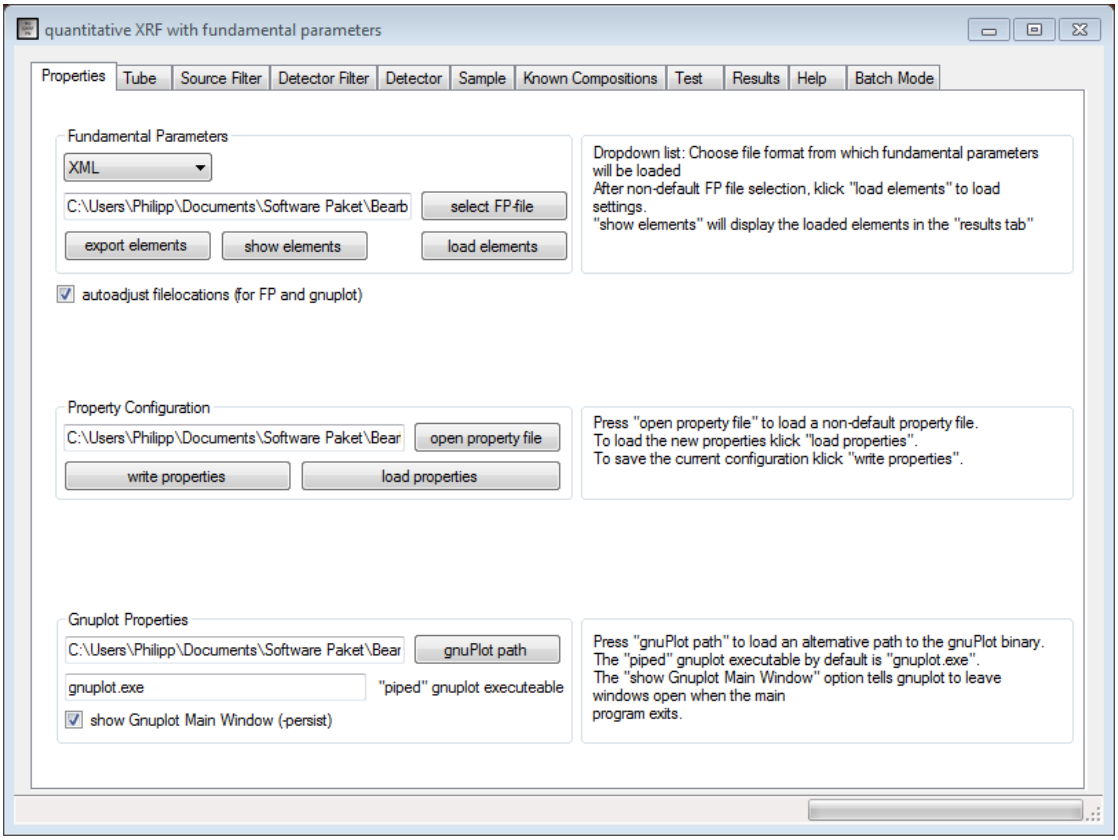

Figure 4.7.: Properties tab of BGQXRFPN.

4.2.1. A quick guide to create a property file within BGQXRF

Follow these steps to quickly create a *property file* for the use in batch mode:

1. Set all parameters of the tube, filters, detector and the sample
2. Switch to the *Properties tab* and select *write properties*
3. Select filename and file path and click the *save* button of the file dialog

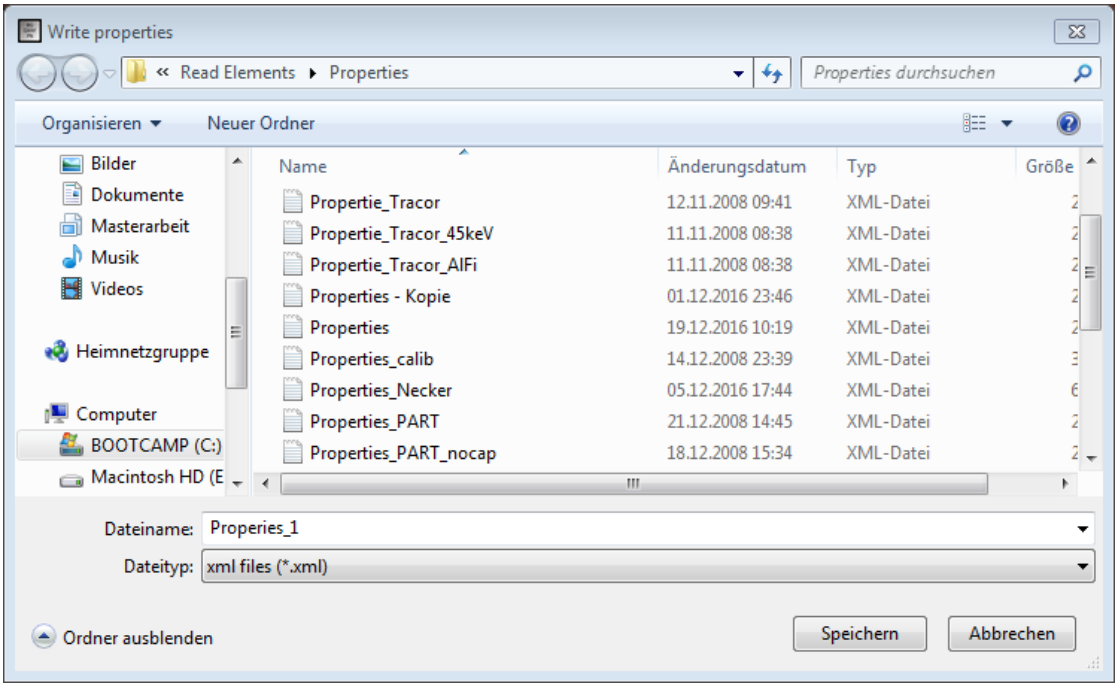

Figure 4.8.: Writing properties of BGQXRFPN to a file.

4.3. Editing with an XML editor

The second way of creating a *property file* provides more possibilities of settings which can be made. Therefore an XML editor needs to be installed. A free open-source choice would be *XML Notepad 2007* which will be discussed in this chapter. [17]

XML Notepad 2007 provides an interface with two panes which allow to easily edit an XML file. Its left structure pane lists the structure of a *Properties.xml* file with every root element (e.g. gnuplot_folder) and child element (e.g. Composition). The right pane represents the value pane consisting of textboxes. They can be changed by typing corresponding values to a root or child element.

To select a specific root or child element, one has to highlight it. The corresponding textbox for value input will be marked.

Adding a new element is done by right-clicking another element and selecting *duplicate*. Names and properties of the copy can be changed.

4.3.1. A quick guide to create a property file within XML Notepad 2007

1. Open XML Notepad 2007
2. Open an already existing *property file* (e.g. Properties.xml) and save it with a different name
3. Change content and values of root and child elements
4. Confirm changes by saving the file

4.4. Loading a property file

Using a *property file* can be helpful while using different measurement setups or while using the *batch mode*. Every setting within the BGQXRFPN can be changed quickly by loading a pre-configured *property file* after program start. Therefore the *Properties tab* has to be opened. In the *Property Configuration* section a specific file can be imported by clicking *open property file* (Fig. 4.9). After selecting a new *property file*, one has to load the new file by clicking *load properties* in the *properties tab* of the software package. This action will automatically set all parameters and settings within BGQXRFPN according to the input file. If no error occurs, all settings are loaded and can be checked by switching tabs.

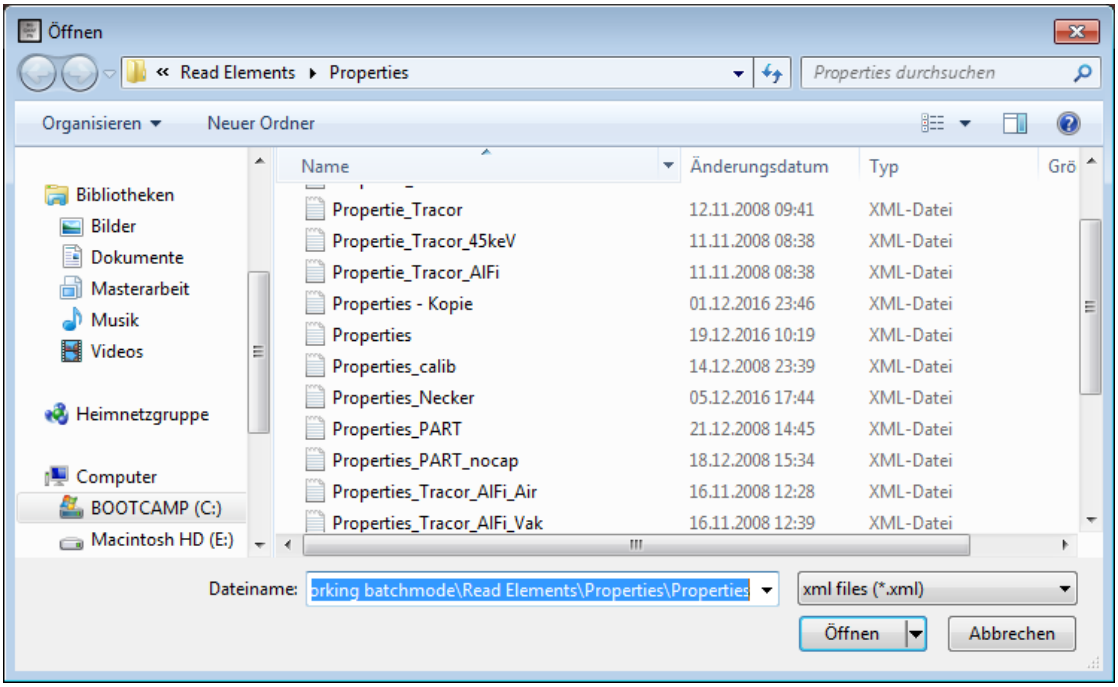

Figure 4.9.: File dialog of BGQXRFPN to select a *property file*. All default *property files* are stored for example in C:\...\Properties.

5. Validation of the BGQXRFPN software package

In the course of this thesis, several measurements were performed to verify the functionality and the reliability of the BGQXRFPN software package. The verification included various brass and bronze standards and one glass standard. Data sheets of the reference materials are given in the appendix. The measurements were performed on the *TRACOR Spectrace 5000* under different conditions depending on the sample and filter method.

The following setups were tested:

- Brass and bronze standards
  - 50 μm palladium filter, 4 mm collimator, air
  - 127 μm aluminium filter, 4 mm collimator, air
- Glass standard
  - No filter, 1 mm collimator, vacuum

During the measurements with a 50 μm palladium source filter the selected tube voltage was 45 kV and the current 0.03 mA. Measurements of the brass and bronze standards with an aluminium filter were performed with a tube voltage of 35 kV and a current of 0.01 mA. The measurement time for the bronzes was 300 seconds each. The glass standard was measured for 1000 seconds with 15 kV tube voltage, 0.3 mA without a filter and under vacuum conditions. All bronze and brass standards were measured three times each, the glass standard was measured twice.

The evaluation of the measurements was done in the AXIL software package with decoupled K_α- and K_β-lines (Cu-K_α and Zn-K_α). Example spectra are shown in figures 5.3 and 5.4.

The results of the aluminium filtered Standard Reference Materials (1103,1107 and 1108) were compared with those of Bernhard Grossmayer (BG value), which were measured with a different collimator (1 mm) and a different tube current (0,08 mA), given in [1]. The deviation Δ between measured and nominal values were also included into this documentation.

Figure 5.1.: Example setup of a TRACOR Spectrace 5000 EDXRF spectrometer [18].

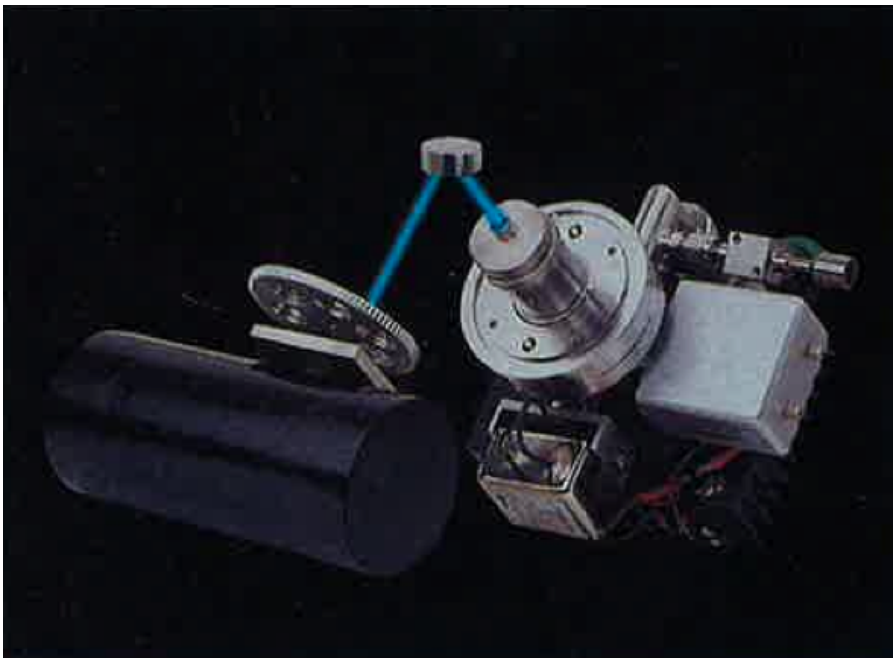

Figure 5.2.: Main components of the TRACOR Spectrace 5000 XRF spectrometer. X-Rays emitted by the sample are getting detected inside a cryogenically cooled, lithium drifted silicon detector. Cooling of the Si(Li) detector can be accomplished with liquid nitrogen or electrically, depending on the sample and setup requirements. [18]

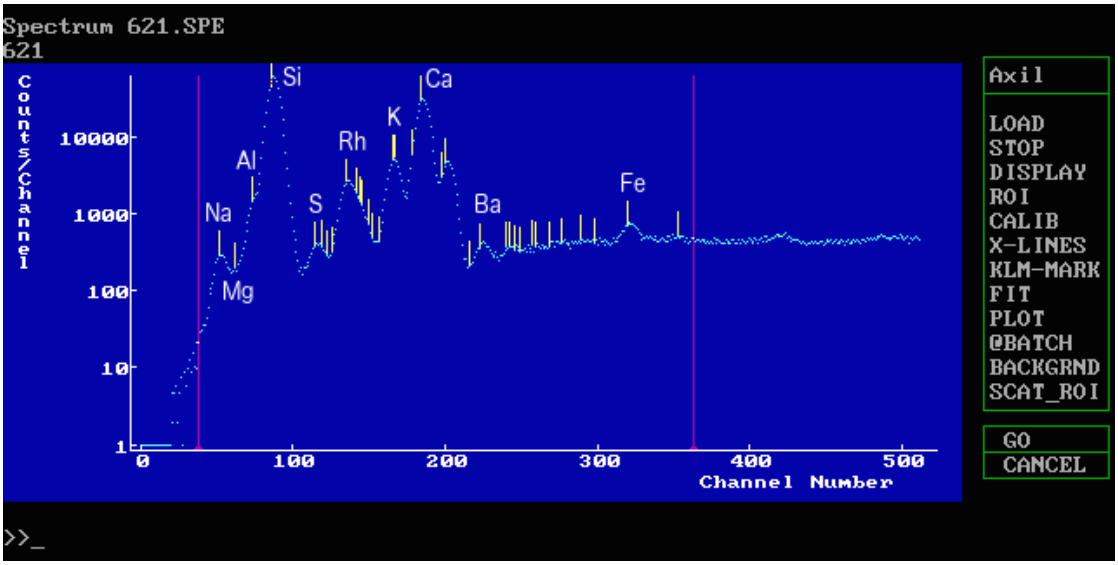

Figure 5.3.: Unfitted spectrum of the Standard Reference Material 621 evaluated in AXIL. The region of interest (ROI) was set between 0.7 keV and 7.3 keV.

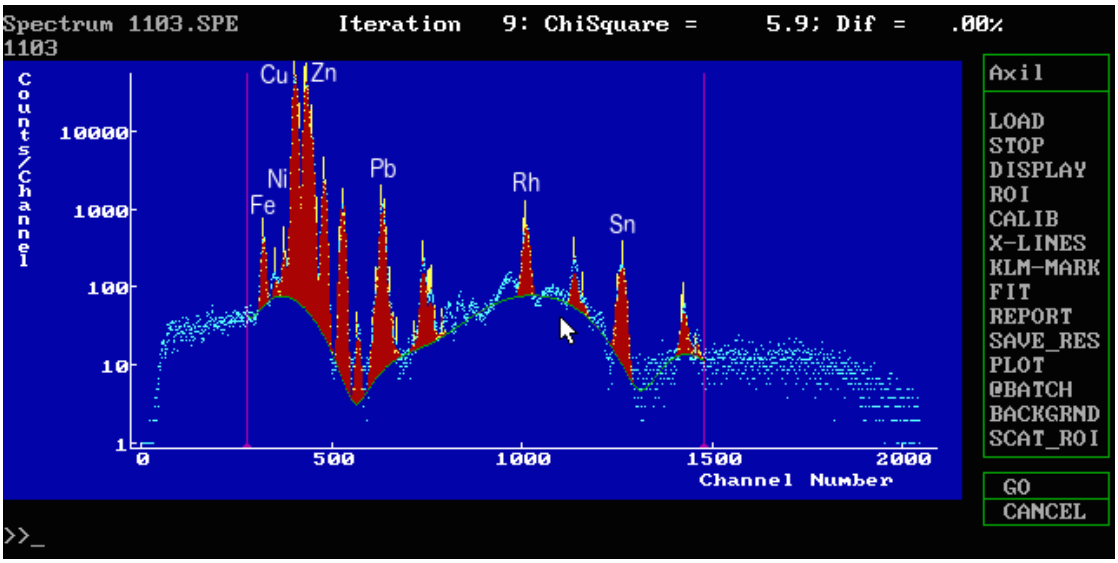

Figure 5.4.: Evaluated spectrum of the Standard Reference Material 1103. The background was fitted with an orthogonal polynomial background model with an order of 12. The region of interest (ROI) was set between 5.6 keV and 29.6 keV to include all peaks of interest.

5.0.1. Measurement of the Standard Reference Material 1103

Palladium filtered

Element	Line	Nominal value	Determined value	Counts	Δ
Fe	Ka	0.26%	0.44 ± 0.01%	4339	0.18%
Ni	Ka	0.15%	0.22 ± 0.02%	3044	0.07%
Cu	Ka	59.27%	59.09 ± 0.07%	667864	-0.18%
Zn	Ka	35.72%	34.98 ± 0.04%	521323	-0.74%
Sn	Ka	0.88%	0.89 ± 0.01%	4029	0.01%
Pb	La	3.73%	4.37 ± 0.03%	16161	0.64%

Table 5.1.: Sample 1103 measured at 45 kV and 0.03 mA with a 50 μm palladium source filter and a 4 mm collimator.

Aluminium filtered

Element	Line	Nominal	BG	Determined value	Counts	Δ
Fe	Ka	0.26%	0.23%	0.41 ± 0.01%	4835	0.15%
Ni	Ka	0.15%	0.14%	0.24 ± 0.01%	3561	0.09%
Cu	Ka	59.27%	59.26%	59.22 ± 0.01%	681378	-0.05%
Zn	Ka	35.72%	35.68%	35.30 ± 0.03%	482575	-0.42%
Sn	Ka	0.88%	1.56%	0.95 ± 0.04%	1206	0.07%
Pb	La	3.73%	3.14%	3.89 ± 0.01%	9682	0.16%

Table 5.2.: Sample 1103 measured at 35 kV and 0.01 mA with a 127 μm aluminium source filter and a 4 mm collimator.

5.0.2. Measurement of the Standard Reference Material 1107

Palladium filtered

Element	Line	Nominal value	Determined value	Counts	Δ
Fe	Ka	0.04%	0.17 ± 0.01%	1900	0.13%
Ni	Ka	0.10%	0.20 ± 0.01%	2943	0.10%
Cu	Ka	61.20%	61.39 ± 0.10%	710524	0.19%
Zn	Ka	36.30%	36.87 ± 0.08%	561253	0.57%
Sn	Ka	1.04%	1.12 ± 0.01%	5093	0.08%
Pb	La	0.18%	0.26 ± 0.01%	889	0.08%

Table 5.3.: Sample 1107 measured at 45 kV and 0.03 mA with a 50 μm palladium source filter and a 4 mm collimator.

Aluminium filtered

Element	Line	Nominal	BG	Determined value	Counts	Δ
Fe	Ka	0.04%	0.01%	0.14 ± 0.02%	1851	0.10%
Ni	Ka	0.10%	0.08%	0.17 ± 0.02%	2706	0.07%
Cu	Ka	61.20%	60.79%	61.30 ± 0.06%	715253	0.10%
Zn	Ka	36.30%	37.09%	36.98 ± 0.03%	512287	0.68%
Sn	Ka	1.04%	1.86%	1.16 ± 0.03%	1507	0.12%
Pb	La	0.18%	0.17%	0.25 ± 0.02%	595	0.07%

Table 5.4.: Sample 1107 measured at 35 kV and 0.01 mA with a 127 μm aluminium source filter and a 4 mm collimator.

5.0.3. Measurement of the Standard Reference Material 1108

Palladium filtered

Element	Line	Nominal value	Determined value	Counts	Δ
Mn	Ka	0.03%	0.01 ± 0.00%	38	-0.02%
Fe	Ka	0.05%	0.18 ± 0.01%	1990	0.13%
Ni	Ka	0.03%	0.10 ± 0.01%	1457	0.07%
Cu	Ka	64.90%	65.10 ± 0.05%	756608	0.20%
Zn	Ka	34.35%	34.10 ± 0.03%	523367	-0.25%
Sn	Ka	0.79%	0.42 ± 0.00%	1884	-0.37%
Pb	La	0.05%	0.10 ± 0.00%	339	0.05%

Table 5.5.: Sample 1108 measured at 45 kV and 0.03 mA with a 50 μm palladium source filter and a 4 mm collimator.

Aluminium filtered

Element	Line	Nominal	BG	Determined value	Counts	Δ
Mn	Ka	0.03%	0.00%	0.01 ± 0.00%	69	-0.02%
Fe	Ka	0.05%	0.02%	0.17 ± 0.00%	2230	0.12%
Ni	Ka	0.03%	0.04%	0.11 ± 0.00%	1792	0.08%
Cu	Ka	64.90%	64.78%	64.93 ± 0.03%	757861	0.03%
Zn	Ka	34.35%	34.35%	34.20 ± 0.05%	476420	-0.15%
Sn	Ka	0.79%	0.76%	0.45 ± 0.02%	585	-0.34%
Pb	La	0.05%	0.05%	0.14 ± 0.01%	327	0.09%

Table 5.6.: Sample 1108 measured at 35 kV and 0.01 mA with a 127 μm aluminium source filter and a 4 mm collimator.

5.0.4. Measurement of the ATI bronze standard 90/4/2/4 (Cu/Pb/Ag/Sn)

Palladium filtered

Element	Line	Nominal value	Determined value	Counts	Δ
Cu	Ka	90.00%	88.47 ± 0.01%	841648	-1.53%
Ag	Ka	2.00%	2.22 ± 0.02%	9110	0.22%
Sn	Ka	4.00%	4.35 ± 0.02%	17751	0.35%
Pb	La	4.00%	4.96 ± 0.04%	17644	0.96%

Table 5.7.: Sample 90/4/2/4 measured at 45 kV and 0.03 mA with a 50 μm palladium source filter and a 4 mm collimator.

Aluminium filtered

Element	Line	Nominal value	Determined value	Counts	Δ
Cu	Ka	90.00%	88.50 ± 0.13%	892818	-1.50%
Ag	Ka	2.00%	2.36 ± 0.06%	7574	0.36%
Sn	Ka	4.00%	4.63 ± 0.24%	5457	0.63%
Pb	La	4.00%	4.51 ± 0.05%	11202	0.51%

Table 5.8.: Sample 90/4/2/4 measured at 35 kV and 0.01 mA with a 127 μm aluminium source filter and a 4 mm collimator.

5.0.5. Measurement of the ATI bronze standard 79.5/12/0.5/8 (Cu/Pb/Ag/Sn)

Palladium filtered

Element	Line	Nominal value	Determined value	Counts	Δ
Cu	Ka	79.50%	78.50 ± 0.07%	729409	-1.00%
Ag	Ka	0.50%	0.53 ± 0.03%	2215	0.03%
Sn	Ka	8.00%	8.13 ± 0.09%	33098	0.13%
Pb	La	12.00%	12.84 ± 0.04%	52593	0.84%

Table 5.9.: Sample 79.5/12/0.5/8 measured at 45 kV and 0.03 mA with a 50 μm palladium source filter and a 4 mm collimator.

Aluminium filtered

Element	Line	Nominal value	Determined value	Counts	Δ
Cu	Ka	79.50%	79.32 ± 0.02%	809117	-0.18%
Ag	Ka	0.50%	0.55 ± 0.04%	1783	0.05%
Sn	Ka	8.00%	8.31 ± 0.04%	9702	0.31%
Pb	La	12.00%	11.82 ± 0.01%	33198	-0.18%

Table 5.10.: Sample 79.5/12/0.5/8 measured at 35 kV and 0.01 mA with a 127 μm aluminium source filter and a 4 mm collimator.

5.0.6. Measurement of the Standard Reference Material 621

Due to the limitations of the calculation of oxides within the BGQXRFPN software package, the Standard Reference Material 621 was used for validation. The oxides of this reference material which were taken into account by the software sum up to 99.91%. The measurements were performed under vacuum conditions with a 1 mm collimator, 15 kV tube voltage, 0.3 mA tube current, and a measurement time of 1000 seconds.

The discrepancy between nominal and measured values in Table 5.11 can be explained by the unknown detector efficiency, the exact values of the contact layer thickness, and the inactive layer thickness, as well as the quality of the vacuum used during the measurements. Contamination of the sample with elements and compositions similar to the constituents of the Standard Reference Material 621 can also not be ruled out. An example spectrum of the glass standard is shown in Fig. 5.3.

Element	Line	Nominal value	Determined value	Counts	Δ
Na2O	Ka	12.74%	4.36 ± 0.05%	2291	-8.38%
MgO	Ka	0.27%	0.66 ± 0.04%	1158	0.39%
SiO2	Ka	71.13%	67.28 ± 0.15%	584584	-3.85%
K2O	Ka	2.01%	3.42 ± 0.01%	49343	1.41%
CaO	Ka	10.71%	20.59 ± 0.01%	316766	9.88%
Fe2O3	Ka	0.04%	0.15 ± 0.00%	4419	0.11%
BaO	La	0.12%	0.22 ± 0.00%	1277	0.10%
SO3	Ka	0.13%	0.11 ± 0.00%	1684	-0.02%
Al2O3	Ka	2.76%	3.21 ± 0.04%	14163	0.45%

Table 5.11.: Sample 621 measured at 15 kV and 0.3 mA with a 1 mm collimator.

6. Conclusion

The aim of this Master's thesis was to improve and expand the functionality of the BGQXRF software package created by Bernhard Grossmayer in 2009 [1]. Besides major bug fixes, most of the implemented changes were related to the user interface of the software package. A new report format was designed and a batch mode for automated calculation of *.ASR files was implemented. For a better user experience quick tips, a general help page and setup sketches were included into the new BGQXRFPN software package.

Validation, requirement testing and reliability testing was performed by measuring several brass and bronze standards, and by measuring a glass standard on a TRACOR Spectrace 5000 EDXRF spectrometer.

The measurement results of the Standard Reference Materials 1103, 1107, and 1108 are in good agreement with the nominal values. The deviations between measured and nominal values are below 1%, independent from the filter method. The ATI bronze standards 90/4/2/4 and 79.5/12/0.5/8 display slightly bigger deviations in the measurement of Cu.

Validation of the glass standard (Standard Reference Material 621) reaches the limits of the BGQXRFPN software package. Due to the unknown detector efficiency, the contact layer thickness, and the inactive layer thickness of the TRACOR Spectrace 5000 EDXRF spectrometer the discrepancy between nominal and measured values could be explained. The quality of the vacuum could also play a role in the measured deviations. The most problematic compositions in evaluation of the Standard Reference Material 621 turned out to be Na_2O, CaO, and SiO_2.

In summary, the analysis of brass and bronze standards can be performed quite accurately within the BGQXRFPN software package in combination with a TRACOR Spectrace 5000 EDXRF spectrometer and the AXIL software package. The analysis and calculation of glass standards could be improved by selecting different detector types, detector setups, and further investigation of detector characteristics in order to achieve reliable results.

A. Appendix

A.1. Standard Reference Material 1103

U. S. Department of Commerce
John T. Connor, Secretary
National Bureau of Standards
A. V. Astin, Director

Certificate of Analysis

Standard Reference Material 1103
Free-Cutting Brass

(Wrought)

ANALYST	COPPER Electrolytic	ZINC ZnS-ZnO	LEAD Weighed as PbO_2	IRON Photometric	TIN $SnCl_2$-KIO_3	NICKEL Photometric	PHOSPHORUS Photometric
1	59.28	35.75	[a]3.65 3.74	[b]0.26	[c]0.88	[d]0.16	[e]0.003
2	59.26	[f]35.72	3.73 [g]3.67	[h].26	[i].89	[j].15	[k].003
3	59.24	[f]35.69	3.79	[m].23	[n].88	[o].14	
4	59.29		3.79	.28	[p].89 [q].86	[o].15	[r].003
Average	59.27	35.72	3.73	0.26	0.88	0.15	0.003

[a] Weighed as $PbMoO_4$.
[b] Orthophenanthroline method.
[c] Tin reduced with cast lead and titrated with KIO_3 standardized with high-purity tin.
[d] Dimethylglyoxime method.
[e] Phosphomolybdenum blue method.
[f] See ASTM Method E 36-45.
[g] Polarographic method.
[h] Iron as chloride extracted with isopropyl ether and determined photometrically with thiocyanate.
[i] Tin reduced with iron and titrated with KIO_3. See ASTM Method E 36-45.
[j] Copper separated by electrolysis. Nickel dimethylglyoxime complex extracted in $CHCl_3$ and photometered.
[k] Molybdivanadophosphoric acid method. See ASTM Method E 62-56.
[l] Sodium ethylenediaminetetraacetate titration.
[m] Dipyridyl method.
[n] Tin separated as metastannic acid, ignited, and SnO_2 volatilized with NH_4I.
[o] Dimethylglyoxime-gravimetric method.
[p] SnO_2-gravimetric method.
[q] Tin titrated with iodine.
[r] Ammonium phosphomolybdate-gravimetric method.

SAMPLE CONDITION.—The wrought sample was prepared from material above the chill-cast samples. Strips of this material were forged, fully annealed, and finished to the sample size of 1¼ in. disk ¾ in. thick.

HOMOGENEITY.—Lead was found to be segregated in the alloy, with deviations of ±0.10 percent from the average value. Metallographic studies, and optical-emission and chemical analyses indicate the homogeneity to be satisfactory for the other elements.

INTENDED USE.—The sample is one of three compositions in a graded series for free-cutting brass in wrought and cast form for application in optical-emission and x-ray spectroscopic analysis. The chill-cast standards are designed for calibration in the analysis of samples prepared in the same manner. Because of the unidirectional solidification, samples prepared by other casting techniques may result in considerable bias.

Details on the preparation and use of the materials can be found in National Bureau of Standards Miscellaneous Publication 260-2, Preparation of NBS Copper-Base Spectrochemical Standards by R. E. Michaelis, LeRoy L. Wyman, and Richard Flitsch. Details on the methods of chemical analysis can be found in National Bureau of Standards Miscellaneous Publication 260-7, Methods for the Chemical Analysis of NBS Copper-Base Spectrochemical Standards by R. K. Bell.

List of Analysts

1. R. K. Bell and E. E. Maczkowske, Division of Analytical Chemistry, National Bureau of Standards.
2. A. E. LaRochelle, Elsie M. Penner, C. H. McMaster and W. R. Inman, Department of Mines and Technical Surveys, Mines Branch, Ottawa, Ontario, Canada.
3. Albert C. Holler, Twin City Testing and Engineering Laboratory, Inc., St. Paul, Minn.
4. Frederick V. Schatz and R. E. Hahn, Metal Physics Department, Revere Copper and Brass, Inc., Rome, N. Y.

WASHINGTON, D. C.
August 13, 1965

W. Wayne Meinke, Chief
Office of Standard Reference Materials.

A.2. Standard Reference Material 1107 and 1108

U. S. Department of Commerce
Malcolm Baldrige
Secretary

National Bureau of Standards
Ernest Ambler, Director

Certificate of Analysis

Naval Brass Standards for Optical Emission and Spectroscopic Analysis

NBS No.[1]	1106 C1106	1107 C1107	1108 C1108
Element		Percent	
Cu	59.0_8	61.2_1	64.9_5
Zn	40.0_8	37.3_4	34.4_2
Pb	0.032	0.18	0.063
Fe	.004	.037	.050
Sn	.74	1.04	.39
Ni	.025	0.098	.033
Al	[2]	-----	-----
Mn	.005	-----	.025

The value listed for a certified element is the *present best estimate* of the "true" value based on the results of the analytical program. The value listed is not expected to deviate from the "true" value by more than ± 1 in the last significant figure reported; for a subscript figure, the deviation is not expected to be more than ± 5. Based on the results of homogeneity testing, maximum variations within and among samples are estimated to be less than the uncertainty figures given above.

[1]Size and metallurgical condition: 1100 series are wrought samples 1 1/4 in in diameter 3/4 in thick. C1100 series are chill-cast samples 1 1/4 in square, 3/4 in thick.

[2]Dashes indicate elements present but not certified.

The material for each standard was melted and cast at the Naval Research Laboratory, Washington, D. C. High-purity metals were used either directly or in the preparation of master alloys. Approximately 650-pound heats were melted under a charcoal cover in a high-frequency induction furnace and the molten metal cast on a massive water-cooled plate to provide rapid unidirectional solidification. The casting for each standard was about 27 in in diameter and 3 1/2 in thick.

The material for the chill-cast samples was obtained from the area of the casting nearest the chill-cast face. Samples were finished to a size 1 1/4 in square, 3/4 in thick, and each has the NBS number marked on the face opposite to the chill-cast or test surface. (In addition, a specimen serial number has been placed on one side face.)

The material for the wrought samples was obtained after removal of the chill-cast material and discard of about 3/4 in thickness from the slab top. Strips of this material were forged, fully annealed, and finished to samples 1 1/4 in in diameter, 3/4 in thick.

Washington, D.C. 20234
November 23, 1981
(Revision of Certificates dated 3-29-61, 8-17-62, 11-17-69, and 8-1-79)

(over)

George A. Uriano, Chief
Office of Standard Reference Materials

The homogeneity of the standards material was investigated by metallographic studies and by optical emission and chemical analyses at the National Bureau of Standards; and by optical emission and chemical analyses by Task Group 3, Subcommittee V of ASTM Committee E-2*. The homogeneity was found to be satisfactory.

Samples for chemical analysis were prepared in the form of millings taken from the cross section of the finished samples of both the chill-cast and wrought material. Chemical analyses were made by R. K. Bell and E. E. Maczkowske, Standard Reference Materials Section, National Bureau of Standards, Washington, D. C.; O. P. Case and Mrs. Kathleen M. O'Brien, Anaconda American Brass Company, Waterbury, Conn.; A. E. LaRochelle, E. M. Penner, C. H. McMaster, and W. R. Inman, Department of Mines and Technical Surveys, Mines Branch, Ottawa, Ontario, Canada; and S. C. Richards, Ray Stevens, and Albert Stuever, Mueller Brass Company, Port Huron, Mich.

Caution should be observed in the use of the chill-cast samples in that determinations made on other than the chill-cast or test surface are not recommended because of the unidirectional solidification. Moreover, the chill-cast standards are designed for calibration in the analysis of samples prepared in the same manner. Samples prepared by other casting techniques may result in considerable bias.

*Task Group 3 cooperators:

Bridgeport Brass Co., Bridgeport, Conn., A. W. Young
Chase Brass and Copper Co., Waterbury, Conn., H. J. Smith
Mueller Brass Co., Port Huron, Mich., S. C. Richards
Olin Mathieson and Brass, Inc., Rome, N. Y., F. V. Schatz (Chairman)
The Anaconda American Brass Co., Waterbury, Conn. J. P. Irwin
Titan Metal Mfg. Co., Bellefonte, Pa., W. M. Rumberger

1106

A.3. Standard Reference Material 621

U. S. Department of Commerce
Malcolm Baldrige
Secretary

National Bureau of Standards
Ernest Ambler, Director

National Bureau of Standards

Certificate

Standard Reference Material 621

Soda–Lime Container Glass

(In cooperation with the American Society for Testing and Materials)

This Standard Reference Material is for use in checking chemical methods of analysis and for calibrating optical emission and x-ray spectrometric methods of analysis.

Constituent	Percent by weight	Uncertainty
SiO_2	71.13	0.03
Na_2O	12.74	0.05
CaO	10.71	0.05
Al_2O_3	2.76	0.04
K_2O	2.01	0.03
MgO	0.27	0.03
SO_3	0.13	0.02
BaO	0.12	0.05
Fe_2O_3	0.040	0.003
As_2O_3	0.030	0.001
TiO_2	0.014	0.003
ZrO_2	0.007	0.001

The certified values are the present best estimates of the "true" values based on the results of a cooperative analytical program. At NBS twelve statistically selected samples of the glass were tested for homogeneity by S.D. Rasberry and L. Zinger using x-ray fluorescence spectrometry. Based on their results the variations among samples are estimated to be less than the uncertainties given above.

The overall direction and coordination of the round-robin analysis leading to certification were performed by Paul Close, Chairman of ASTM Subcommittee C-14.02 on Chemical Analysis of Glass and Glass Products.

The technical and support aspects involved in the preparation, certification, and issuance of this Standard Reference Material were coordinated through the Office of Standard Reference Materials by G.W. Cleek, C.L. Stanley, and R.E. Michaelis.

Washington, D.C. 20234
January 21, 1982
(Revision of certificate
dated 3/13/75.)

George A. Uriano, Chief
Office of Standard Reference Materials

(over)

List of Figures

List of Tables

Bibliography

[1] B. Grossmayer, "Softwarepaket zur quantitativen Röntgenfluoreszenzanalyse mittels fundamentaler Parameter unter Verwendung von Röntgenoptiken," Master's thesis, Vienna University of Technology, January 2009.

[2] R. Jenkins, R. Gould, and D. Gedcke, *Quantitative X-Ray Spectrometry*. Marcel Dekker Inc., 1981.

[3] Wikipedia, "Auger effect." https://en.wikipedia.org/wiki/Auger_effect. Last visited 16.2.2017.

[4] L. Meitner, "Über die β-Strahl-Spektra und ihren Zusammenhang mit der γ-Strahlung," *Zeitschrift für Physik*, vol. 11, pp. 35–54, 1922.

[5] Wikipedia, "Bremsstrahlung." https://en.wikipedia.org/wiki/Bremsstrahlung. Last visited 16.2.2017.

[6] H. A. Kramers, "On the Theory of X-Ray Absorption and of the Continuous C-Ray Spectrum," *Phil. Mag. 46*, pp. 836–871, 1923.

[7] Wikipedia, "X-ray tube." https://en.wikipedia.org/wiki/X-ray_tube. Last visited 16.2.2017.

[8] Amptec Inc., "CdTe Application Note: Characterization of X-ray Tubes." http://amptek.com. Last visited 4.5.2017.

[9] Wikipedia, "Synchrotron." https://de.wikipedia.org/wiki/Synchrotron. Last visited 17.2.2017.

[10] N. Zöger, *Micro X-ray Fluorescence Analysis and Micro- Tomography of Human Bone and Tissue*. PhD thesis, Vienna University of Technology, May 2005.

[11] X. Gruber, "Röntgenfluoreszenzanalyse österreichischer Weine und zugehöriger Bodenproben," Master's thesis, Vienna University of Technology, 2005.

[12] Amptec Inc., "XR-100SDD Silicon Drift Detector (SDD)." http://amptek.com. Last visited 13.3.2017.

[13] European Space Agency. http://sci.esa.int. Last visited 13.3.2017.

[14] H. Wiederschwinger, *Eine universelle Beschreibung der Röntgenröhrenspektren für die quantitative Röntgenfluoreszenzanalyse*. PhD thesis, Vienna, 1990.

[15] G. Love, M. G. Cox, and V. Scott, "On the Theory of X-Ray Absorption and of the Continuous C-Ray Spectrum," *J. Phys. D: Appl. Phys.*, no. 11,30, 1978,1980.

[16] H. Ebel, "X-ray tube spectra," *X-Ray Spectrometry*, vol. 28, pp. 255–266, July/August 1999.

[17] Microsoft, "XML Notepad." http://xmlnotepad.codeplex.com, 2015. Last visited 4.1.2017.

[18] Spectrace Instruments, "TRACOR Spectrace 5000 XRF Spectrometer." Commercial brochure, 1995, actual Thermo Fisher Scientific.

[19] Wikipedia, "Semiconductor detector." https://en.wikipedia.org/wiki/Semiconductor_detector. Last visited 3.3.2017.

[20] R. Jenkins, *X-Ray Fluorescence Spectrometry*. New York: John Wiley & Sons, Inc., 2nd ed., 1999.

[21] Wikipedia, "pin-Diode." https://de.wikipedia.org/wiki/Pin-Diode. Last visited 3.5.2017.

[22] B. Beckhoff, B. Kanngießer, N. Langhoff, R. Wedell, and H. Wolff, *Handbook of Practical X-Ray Fluorescence Analysis*. Berlin Heidelberg: Springer, 2006.